NTIA Report TR-15-513

Effect of Broadband Radio Service Reallocation on 2900–3100 MHz Band Marine Radars: Background

Robert Achatz
Paul McKenna
Roger Dalke
Nicholas DeMinco
Frank Sanders
John Carroll

report series

U.S. DEPARTMENT OF COMMERCE • National Telecommunications and Information Administration

NTIA Report TR-15-513

Effect of Broadband Radio Service Reallocation on 2900–3100 MHz Band Marine Radars: Background

Robert Achatz
Paul McKenna
Roger Dalke
Nicholas DeMinco
Frank Sanders
John Carroll

U.S. DEPARTMENT OF COMMERCE

April 2015

DISCLAIMER

Certain commercial equipment and materials are identified in this report to specify adequately the technical aspects of the reported results. In no case does such identification imply recommendation or endorsement by the National Telecommunications and Information Administration, nor does it imply that the material or equipment identified is the best available for this purpose.

CONTENTS

LIST OF FIGURES

LIST OF TABLES

ACRONYMS

3GPP 3rd Generation Partnership Project

APD Amplitude probability distribution

AWGN Additive white Gaussian noise

BPF Bandpass filter

BRS Broadband radio service

BS Base station

BW Bandwidth

CFAR Constant false alarm rate

CW Continuous wave

dB Decibel

dBi Decibels relative to the gain of an isotropic antenna

dBm Decibels relative to a milliwatt

dBsm Decibels relative to a square meter

dBW Decibels relative to a watt

DOD Department of Defense

EIRP Effective isotropic radiated power

ETSI European Telecommunications Standards Institute

FDD Frequency division duplex

FDR Frequency dependent rejection

FE Front-end

FEF Front-end filter

FS Free space

GHz Gigahertz

GN Gaussian noise

Hz Hertz

IEC International Electrotechnical Committee

IEEE Institute of Electrical and Electronics Engineers

IF Intermediate frequency

INR Interference to noise power ratio

IPC Interference protection criteria

ITM Irregular terrain model

ITS Institute for Telecommunication Sciences

ITU International Telecommunication Union

ITU-R ITU Radiocommunication Sector

km Kilometer

kHz kilohertz

LNA Low-noise amplifier

LNFE Low-noise front-end

LTE Long Term Evolution

MHz Megahertz

MIMO Multiple-input multiple-output

MSC Maritime Safety Committee

nmi Nautical mile

ns Nanosecond

NTIA National Telecommunications and Information Administration

OFDM Orthogonal frequency division multiplexing

OFDMA Orthogonal frequency division multiple access

OOB Out-of-band

PAM Pulse amplitude modulation

PRF Pulse repetition frequency

PRI Pulse repetition interval

PSD Power spectral density

PSK Phase shift keyed

QAM Quadrature modulation

RCS Radar cross section

RF Radio frequency

RPM Revolutions per minute

SA Spectrum analyzer

SINR Signal to interference plus noise ratio

SNR Signal to noise ratio

SOLAS Safety of life at sea

STC Sensitivity time control

TDD Time division duplex

UMTS Universal Mobile Telecommunications System

UN United Nations

UN/MSC United Nations Maritime Safety Committee

USCG United States Coast Guard

VSA Vector signal analyzer

WGN White Gaussian noise

WiMAX Worldwide interoperability for microwave access

EXECUTIVE SUMMARY

Spectrum reallocation is often necessary to accommodate new services which can potentially increase business productivity and enhance the lives of private citizens. However, reallocating services to bands near those used by incumbent services—or, in some cases, to those same bands—can cause interference to the incumbent service.

Spectrum reallocation can cause interference in radar systems in a number of ways. A system reallocated to a nearby band can introduce unwanted signals into the radar detection bandwidth. Also, a system reallocated to a nearby band can overload the radar receiver front-end and cause gain compression, increased noise power, and intermodulation in the radar detection bandwidth.

The U.S. Coast Guard (USCG) asked the National Telecommunications and Information Administration Institute for Telecommunication Sciences (NTIA/ITS) to investigate effects of reallocation on the 2900–3100 MHz band marine radar service by determining interference protection criteria (IPC) and analyzing strategies for mitigating the interference.

Here we investigate the effects of reallocation to accommodate the broadband radio services (BRS) on the 2900–3100 MHz band marine radar service. The BRS is the next generation of personal communications services which will provide wideband Internet communications to mobile users. Results of our investigations have been assembled into three reports subtitled "Background," "Unwanted Emissions," and "Front-end Overload."

This report provides background information needed to analyze effects of BRS reallocation on 2900–3100 MHz band marine radars. Key topics covered are interference protection criteria (IPC), interference scenario, and the various system and propagation models.

Comprehensive IPC include performance levels, powers, and reliabilities for baseline (interference-free) and allowable degraded conditions. Reliability in this context is determined solely by radio wave propagation path loss variability caused by terrain and atmospheric conditions and is independent of electrical or mechanical malfunction.

The interference scenario consists of a maritime radar target such as a boat or buoy between a network of base stations and a ship with a maritime radar. Magnetron radar and radar target models are derived from the IEC 62388 standard for shipborne radars. BRS system models are derived from WiMAX and LTE standards. Radio wave propagation is modelled with the ITS Irregular Terrain Model (ITM) because of its ability to model path loss variability.

A BRS base station signal was measured and statistically characterized. The signal statistics were found to be nearly Gaussian in the necessary bandwidth and Gaussian in the spurious domain. Statistics in the necessary bandwidth are considered nearly Gaussian because of a slight drop in peak signal levels. The roll-off or out-of-band (OOB) regions between the necessary bandwidth and spurious regions were not measured due to measurement system dynamic range considerations. Pending future measurements, we are assuming OOB emissions are Gaussian as well. Consequently, it is reasonable to model the BRS signal as Gaussian noise. This finding greatly simplifies analysis of interference in marine radars from base station unwanted emissions.

Statistical characterization was done on measurements in a wide bandwidth. However, since the statistics are Gaussian they should also be Gaussian when the BRS signal is filtered to a narrower bandwidth and when any number of BRS signals are added to represent the signal from an aggregate of base stations.

A method for computing aggregate interference power distributions using the radio wave propagation model and Monte Carlo analysis was developed. These distributions are essential for analyzing radar link reliability. Because of the radar antenna's narrow azimuthal beam width, maximum aggregate interference power was found to come from base stations along a line formed by the most closely repetitively-spaced base stations. The aggregate interference power was found to be as much as 6 dB greater than the power from a single base station. Hence it is important that interference analysis be done with an aggregate of base stations.

Although interference path loss variability is usually included in interference analysis, desired path loss variability often is not. In the maritime radar case the desired path is the radar to target path. In devising a method for including radar to target path loss variability into our analysis we found excess signal to noise ratio (SNR) in the radar to target link budgets used for industry acceptance tests. Although this excess SNR could potentially mitigate interference, we found that it is needed to accommodate reductions in target mean radar cross section (RCS) due to changes in target aspect, shape, and construction materials. Consequently we recommend removing the excess SNR by reducing mean RCS prior to interference analysis.

EFFECT OF BROADBAND RADIO SERVICE REALLOCATION ON 2900–3100 MHZ BAND MARINE RADARS: BACKGROUND

Robert Achatz, Paul McKenna, Roger Dalke, Nicholas DeMinco, Frank Sanders, John Carroll[1]

Spectrum reallocations may place broadband radio services (BRS) near spectrum used by 2900–3100 MHz band marine radars. Interference effects from these reallocations include unwanted emissions in the radar detection bandwidth and front-end overload. This report provides background information for subsequent reports that analyze these effects. Interference protection criteria (IPC) are identified, an interference scenario is described, and models for the radar system, BRS system, radar target, and radio wave propagation are presented. The BRS signal is shown to be reasonably emulated by Gaussian noise. A method for determining the aggregate power distribution using a realistic propagation model and Monte Carlo analysis is described. The aggregate power from the base stations was found to be as much as 6 dB more than power from a single base station. Finally a method for incorporating a variable SNR, caused by variable radar to target path loss, into interference analysis is shown.

Keywords: aggregate power, broadband radio service, front-end overload, interference, interference protection criteria, marine radar, radar, radio spectrum engineering, radio wave propagation, signal characterization, unwanted emissions

1 INTRODUCTION

Spectrum reallocation is often necessary to accommodate new services which can potentially increase business productivity and enhance the lives of private citizens. However, reallocating services to bands near those used by incumbent services—or, in some cases, to those same bands—can cause interference to the incumbent service.

Spectrum reallocation can cause interference in radar systems in a number of ways [1], [2], [3], [4]. For example, a system moved to a nearby band can introduce unwanted emissions into the radar detection bandwidth. Also, emissions from a system reallocated to a nearby band can overload the radar receiver front-end (receiver circuits operating at the carrier frequency) and cause gain compression, increased noise power, and intermodulation in the radar detection bandwidth.

The U.S. Coast Guard (USCG) asked the National Telecommunications and Information Administration Institute for Telecommunication Sciences (NTIA/ITS) to investigate effects of

[1]The authors are with the Institute for Telecommunication Sciences, National Telecommunications and Information Administration, U.S. Department of Commerce, Boulder, CO 80305.

spectrum reallocation on the 2900–3100 MHz band marine radar service by determining interference protection criteria (IPC) and analyzing strategies for mitigating the interference.

Results of these investigations are expected to be useful to regulatory and standards bodies which are responsible for developing IPC including the NTIA [5]; the International Telecommunication Union (ITU) [6]; the International Electrotechnical Commission (IEC) [7], which is currently devising IPC tests on behalf of the United Nations Maritime Safety Committee (UN/MSC) [8]; and the Institute of Electrical and Electronics Engineers (IEEE) [9].

In this series of reports we analyze the effects of reallocation to accommodate broadband radio services (BRS) on the 2900–3100 MHz band marine radar service. The BRS is the next generation of personal communications services which will provide wideband Internet communications to mobile users. Spectrum regulators are currently investigating various reallocation strategies to accommodate BRS growth.

Marine radars are used by ships to avoid collisions with objects while traveling in oceans, seas, lakes, and rivers. An example of a marine radar antenna mounted on a ship is shown in Figure 1. Detection of objects, referred to as targets, is often difficult. Even on calm seas, the target can have significant radar cross section (RCS) variation and corresponding reductions in signal power. The target can also be obscured by signal reflections or clutter from waves and precipitation.

These 2900–3100 MHz band radars are often referred to as S-band marine radars. Similar radars that operate in the 9200–9500 MHz band are often referred to as X-band marine radars. The primary advantage of S-band radar signals is that they have less precipitation attenuation than X-band radar signals. This allows S-band radars to detect smaller objects at longer distances in adverse weather conditions. Large ships subject to international safety of life at sea (SOLAS) regulations generally operate with radars in both bands.

BRS providers promise to deliver fast, reliable Internet service to users wherever they are. An example of a BRS base station is shown in Figure 2. Potential unwanted emissions and front-end overload problems in S-band marine radars from BRS base stations were brought to the attention of the International Telecommunication Union in November 2009 by the United Kingdom [10].

Significant amounts of spectrum are needed for widespread BRS use. BRS systems are already operating in the 2500–2690 MHz band. The 3500–3650 MHz band has been evaluated for reallocation [11]. Other reallocations in the 2700–3700 band, currently allocated to a number of radar services as shown in Figure 3, could also affect 2900–3100 MHz band marine radars.

BRS and radar system characteristics are derived from those used by internationally recognized groups. The BRS system is modeled after systems devised by the European Technical Standards Institute (ETSI) Universal Mobile Telecommunications System (UMTS) committee/3rd Generation Partnership Project (3GPP) [12], ITU [13], and the WiMAX Forum [14]. The radar system is modeled after a system devised by the IEC 62388 standard shipborne radar committee [7] for industry acceptance testing.

Figure 1. Marine radar slotted array antenna (white bar) mounted on motor which spins it.

Figure 2. BRS base station.

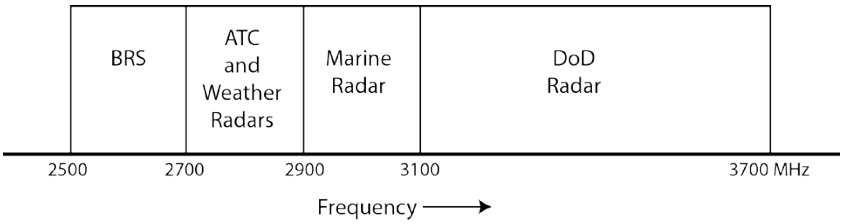

Figure 3. Radio spectrum from 2500 to 3700 MHz with current allocations for air traffic control (ATC), weather, marine, and various Department of Defense (DOD) radar services.

1.1 Unwanted Emissions and Front-end Overload

Figure 4 is a general diagram of the interference scenario. On the left is a network of base stations emitting signals in the direction of the marine radar. The marine radar receives these signals along with its own signal returning from the target. Key components in analyzing the interference include the base station transmitter filter, the radar receiver front-end filter and low-noise amplifier, and the radar signal processor detection filter often referred to as the intermediate frequency (IF) filter.

Figure 5 illustrates four possible outcomes of spectrum reallocation with regard to unwanted emissions and front-end overload. A generic interfering signal power spectral density (PSD), centered at f_i, is depicted by the shaded area. The unwanted emissions are represented as the sloped section of the PSD. The radar receiver front-end and signal processor IF bandwidths are depicted with dashed lines. The radar received signal PSD, centered at f_r, is shown for reference purposes.

In Figure 5(a) the radar receiver is free of interference because the interfering PSD does not introduce unwanted emissions into the radar detection IF bandwidth and the radar front-end bandwidth excludes most of the interfering signal power. In Figure 5(b) the radar receiver has potential interference from unwanted emissions in the radar detection IF bandwidth. In Figure 5(c) the radar receiver has potential interference from the interfering signal in the radar front-end bandwidth. Finally, Figure 5(d) has both interference potentials.

There are a number of ways the interference can be mitigated. Both unwanted emissions and front-end overload can be mitigated by decreasing transmitted power, increasing the distance separation between the base stations and the radar locations, and increasing the frequency separation between the base station and radar center frequencies. Interference from the unwanted emissions can be controlled with the base station transmitter filter. Front-end overload can be prevented with the radar front-end filter.

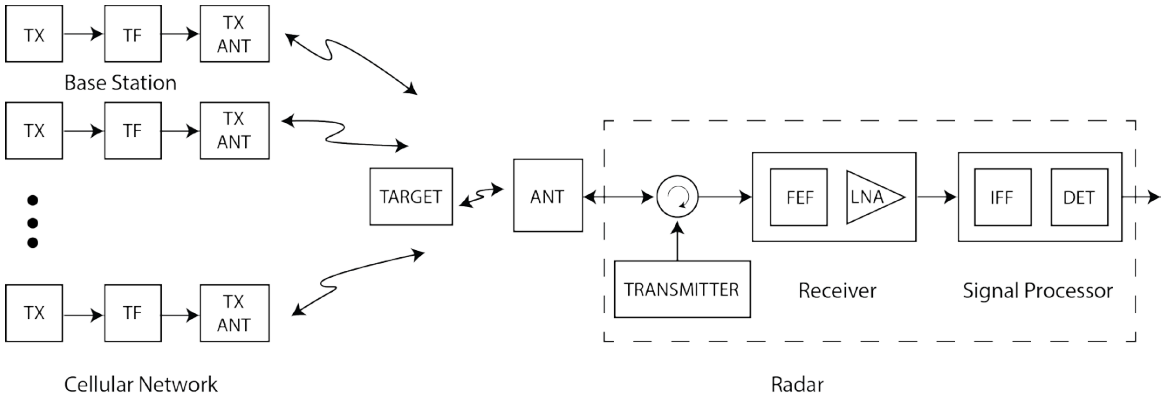

Figure 4. Simplified diagram of BRS base stations and radar equipment showing location of base station transmitter filter (TF) and radar front-end filter (FEF) which mitigate unwanted emissions and front-end overload, respectively. TX represents the BRS transmitter, TX ANT represents the transmit antenna, ANT represents the radar antenna, LNA represents the low-noise amplifier, IFF represents the intermediate frequency filter, and DET represents the threshold detector.

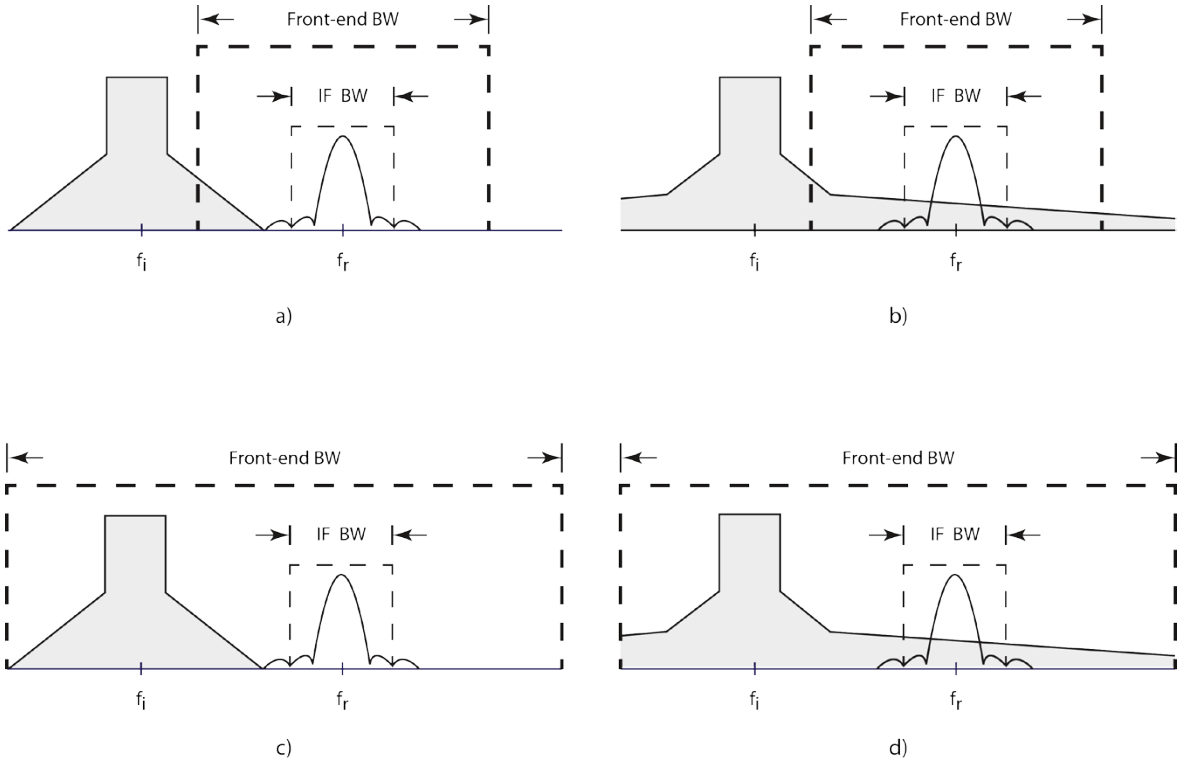

Figure 5. Four possible reallocation scenarios illustrated with interfering and radar PSDs. The interfering PSD is centered around f_i. The radar PSD is centered around f_r. Radar IF and front-end bandwidths are shown with dashed lines. The scenarios are a) no interference, b) potential unwanted emission interference, c) potential front-end overload, and d) potential unwanted emission and front-end overload interference.

1.2 Report Series Organization

Results of our investigations have been assembled into three reports subtitled Background, Unwanted Emissions, and Front-end Overload. This Background report identifies IPC, defines the scenario where interference will be evaluated, and distills the scenario into models for analysis. In addition, three fundamental modeling issues are examined. First, BRS signal statistics are tested to see if the BRS signal can be emulated with a more analytically tractable Gaussian noise process. Second, aggregate power from all base stations in the network is calculated to determine if it is necessary to use the aggregate power as an interference source. Third, we develop a method for incorporating variable radar SNR caused by dynamic atmospheric conditions into our analysis so that we can include scenarios with long radar to target ranges.

The Unwanted Emissions report determines relevant IPC and the distance and frequency separations needed to mitigate interference. Distance separation is analyzed with constant and variable SNRs corresponding to short and long radar to target ranges, respectively. Results are compared to determine worst case conditions. Frequency separation is analyzed using frequency dependent rejection (FDR) which takes the transmitted PSD and the radar receiver IF filters frequency responses into account. We also show how interference can be mitigated by the combination of distance and frequency separation.

The Front-end Overload report determines relevant IPC, front-end filter attenuation, and separation distances needed to prevent overload. IPC are determined from probability of detection measurements with a custom test fixture. Results are compared to commonly used overload metrics such as receiver front-end gain compression which are easier to execute than probability of detection measurements.

2 INTERFERENCE PROTECTION CRITERIA

Marine radars are used to avoid collisions with other objects in the water such as boats or underwater objects marked by buoys. Radar receiver noise and signal reflections or clutter from the sea or precipitation can obscure these objects and thereby contribute to collisions. Engineers design radar systems so that the probability of a collision is reasonably low without placing undue burden on the cost of the radar. Interfering signals can also obscure objects. IPC are needed to keep the probability of collision low while not placing onerous burdens on other systems using the radio spectrum.

IPC are based on measurable performance parameters. Radar manufacturers quantify performance with four principal parameters, i.e., RCS, range, probability of detection ($\mathcal{P}_d$), and probability of false alarm (P_{fa}). As an example [7], a 2900–3100 MHz band marine radar must be able to detect a small boat with a 1.4 m^2 RCS at a range of 5.6 km (3.0 nmi) with a 0.8 $\mathcal{P}_d$ and 10^{-4} P_{fa}.

We have chosen to quantify performance with $\mathcal{P}_d$ at a specific P_{fa} while controlling RCS and range with signal to noise ratio (SNR) so the method can be implemented in the laboratory via conducted measurements. With this approach there are six IPC:

- Baseline performance level:
  The desired probability of detection, $\mathcal{P}_{d,b}$, and probability of false alarm, $\mathcal{P}_{fa,b}$, in the absence of the interfering signal.

- Baseline signal and noise power:
  Signal and noise power required to meet baseline performance level.

- Baseline reliability:
  The probability, $Pr\{P_d > P_{d,b}\}$, that P_d will exceed $P_{d,b}$ at a specified percentage of locations and times. This reliability depends on propagation path loss variability caused by terrain and atmospheric conditions and is independent of electrical or mechanical malfunction.

- Allowable degraded performance level:
  The probability of detection, $\mathcal{P}_{d,a}$, and probability of false alarm, $\mathcal{P}_{fa,a}$, corresponding to the degraded performance allowable in the presence of the interfering signal. To minimize variables, $\mathcal{P}_{fa,a}$ is assumed to be the same as $\mathcal{P}_{fa,b}$. The corresponding allowable degraded performance percentage is a relative measure of degradation.

$$\text{allowable degraded performance percentage} = \left(\frac{\mathcal{P}_{d,b} - \mathcal{P}_{d,a}}{\mathcal{P}_{d,b}}\right) \cdot 100\ \% \qquad (1)$$

- Allowable interference power level:
  The interference power that degrades radar performance from baseline to allowable degraded. The power is dependent on the interfering signal characteristics. As an example the

allowable degraded power level of a Gaussian distributed interfering signal is expected to differ from that of a continuous-wave (CW) interfering signal.

- Allowable reliability:
  The probability, $Pr\{P_d > P_{d,a}\}$, that P_d will exceed $P_{d,a}$ at a specified percentage of locations and times. This reliability depends on propagation path loss variability caused by terrain and atmospheric conditions and is independent of electrical or mechanical malfunction.

3 SCENARIO

3.1 Physical Layout

The physical layout of the radar, target, and base stations are shown in Figure 6. The radar is mounted on a ship and the target the radar is to detect is between the ship and the closest base station. Other base stations are located behind and to the side of the closest base station. The potential for interference in this scenario is enhanced in two ways. First, BRS base station antenna heights can be tall enough to transmit signals over considerable line-of-sight distances. Second, the radar can receive signals from more than one or an aggregate of base stations.

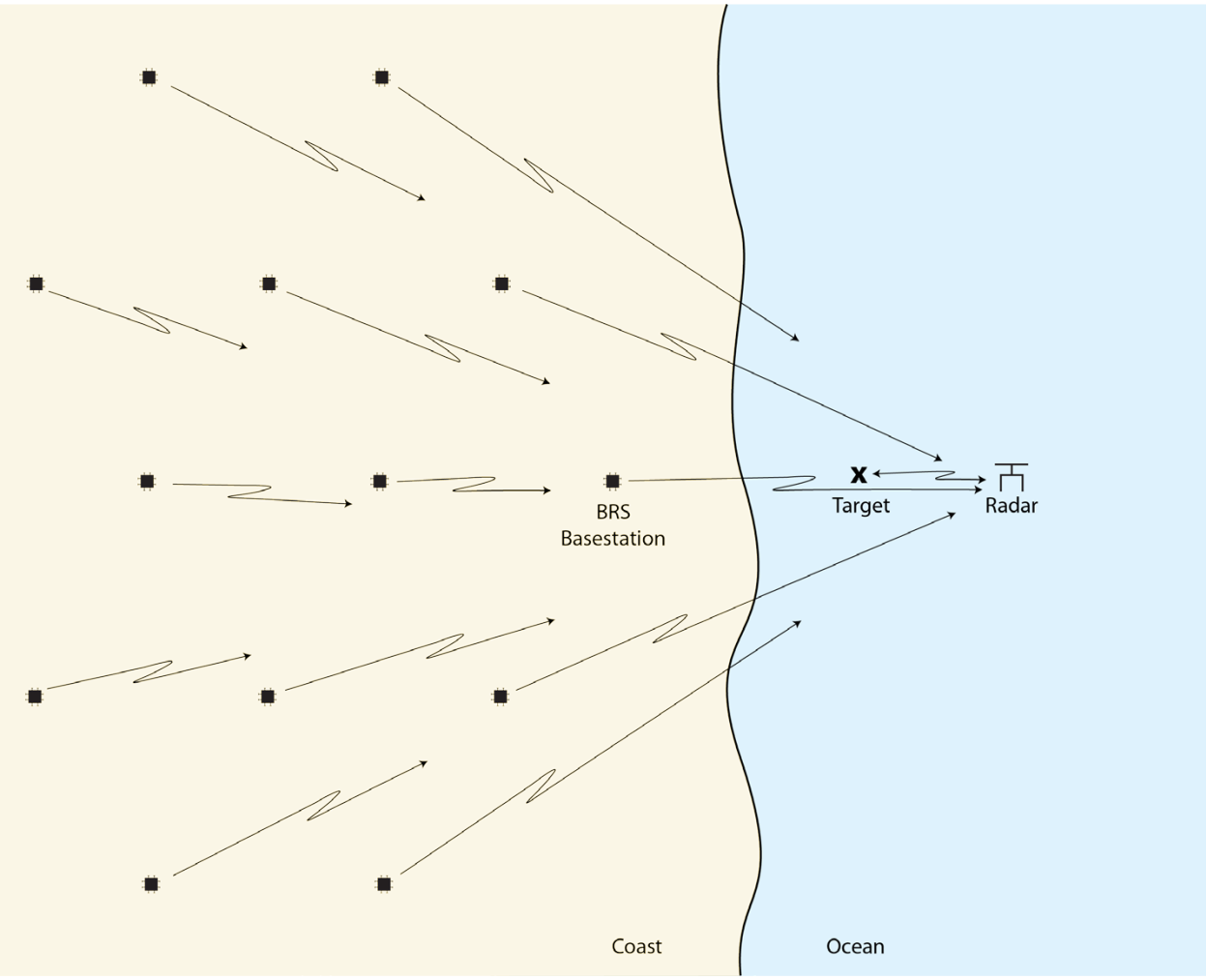

Figure 6. Physical layout showing a network of BRS base stations contributing to the interfering signal power. The interference can cause the radar to not detect the target.

3.2 Weather Conditions

Marine radars operate in all weather conditions. Signals reflected from the waves, rain, and snow present in adverse conditions create clutter that obscures signals returned from the target. The IEC 62388 standard has tests with [15] and without clutter [16]. Rain clutter tests are identical to tests without rain clutter except that range requirements are reduced. Sea clutter tests are performed with an additional short range test that reduces probability of detection requirements as wave height increases.

3.3 Radar System

The radar system is assumed to be a conventional magnetron radar modeled after the radar used in the IEC 62388 standard [17], [18]. The block diagram of the radar in Figure 7(a) shows that it is comprised of a rotating antenna, rotary joint, transmission line, circulator, transmitter, receiver, signal processor, data processor, and display.

The radar antenna is horizontally polarized. It has a narrow azimuthal beam width, necessary for discriminating against targets that are close in bearing. It also has a wide elevation beam width so that the radar can detect near and far targets and accommodate ship rocking.

Installation is assumed to be down-mast, i.e., the antenna and rotary joint are installed in a radome at a high, unobstructed location such as the top of a mast and the electronics are installed at a lower location such as the bottom of the mast. A transmission line carries signals between the antenna and the circulator. The circulator directs signals from the transmitter to the antenna and from the antenna to the receiver while isolating the receiver from the strong transmitted signals.

The radar signal is created by modulating the output of a magnetron oscillator with a train of periodic rectangular pulses. Typically short, medium, and long pulse widths are available. Pulse widths and corresponding pulse repetition frequencies used depend on a number of factors including target range, target resolution, and clutter conditions.

The purpose of the receiver is to convert the received signal to the intermediate frequency (IF). As shown in Figure 7(b), the receiver contains the limiter, front-end filter (FEF), low-noise front-end (LNFE), filter, and amplifier. The LNFE has a low-noise amplifier (LNA) and frequency down-conversion mixer. The circulator is not ideal and passes a portion of the transmitted signal's power to the receiver. The limiter prevents the LNFE from being damaged by the transmitted signal. The FEF protects the LNFE from overload. The LNFE amplifies the received signal and multiplies it by the local oscillator continuous wave (CW) signal which shifts it to the IF. The filter and amplifier after the LNFE represent initial stages of IF filtering and amplification.

The signal processor extracts target range from the IF signal. Details of the signal processor block are shown in Figure 7(c). It consists of a detection or final IF filter which we refer to more generally as the IF filter, envelope detector, non-coherent integrator, and threshold detector. The signal processor filters and then integrates the pulses to increase SNR. In magnetron radars, the IF filter is not always matched to the transmitted pulse shape. For a rectangular pulse this means

that the IF filter equivalent noise bandwidth is not always the reciprocal of the transmitted pulse width.

Detection is accomplished by comparing the integrated pulse envelope to a threshold determined by the P_{fa} and the constant false alarm rate (CFAR) function. The data processor uses range data provided by the signal processor for tasks such as target tracking.

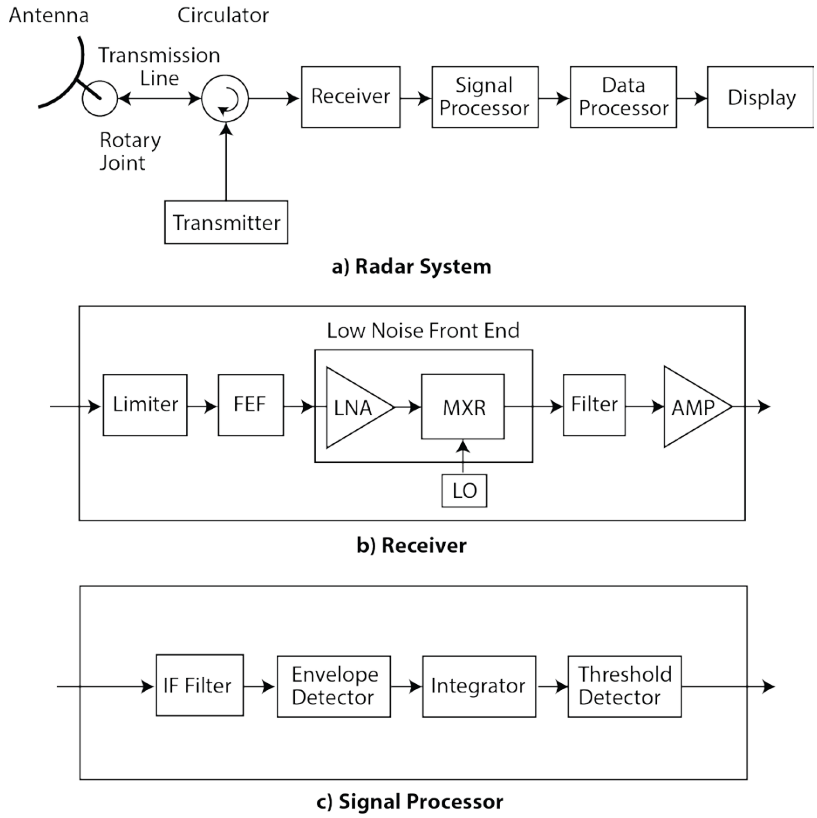

Figure 7. Radar equipment components. The top diagram (a) shows the major radar system functional blocks, the middle diagram (b) shows components in the receiver block, and the bottom diagram (c) shows components in the signal processor block. FEF represents the front-end filter, LNA represents the low-noise amplifier, MXR represents the mixer, LO represents the local oscillator, and AMP represents the amplifier.

3.4 BRS System

The BRS system is modeled after those described in the ETSI UMTS [12], 3GPP, ITU [13], and WiMAX Forum [14] standards. The base stations within the system work cooperatively as a cellular network. In this work we are only concerned about the BRS base station transmitter whose simplified block diagram is shown in Figure 8.

In the block diagram, the baseband modulator block converts bits to either phase shift keyed (PSK) or quadrature amplitude modulated (QAM) symbols [19]. The orthogonal frequency division multiple access (OFDMA) block serializes the modulated symbols, performs an inverse

Fourier transform operation, adds a cyclic prefix, and applies a window that shapes the spectrum. OFDMA is a multi-user implementation of orthogonal frequency division multiplexing (OFDM).The RF modulator and amplifier blocks convert the signal to a higher frequency and power, respectively, for transmission. The transmitter filter block reduces unwanted emissions prior to transmission out of the antenna.

The base station antennas are typically mounted on a tower or building high above ground level. The base station antenna azimuth beam width divides the coverage areas into wedge shaped sectors. The elevation beam width is narrow and can be tilted down to decrease interference in other base stations. The signal is transmitted with 45˚ slant-angle cross polarization. Multiple antennas within each sector are used to transmit independent data streams for multiple-input multiple-output (MIMO) signal processing to enhance performance.

The frequency allocation or channel that accommodates the signal is defined by its center frequency and bandwidth; the bandwidth ranges from 1.25 to 20 MHz. BRS channels are reused by multiple base station sectors to boost spectrum efficiency The same BRS channel can be reused by all base stations and sectors. Under some circumstances, all channels can be used by the same sector [20].

The signal's temporal characteristics are dependent, amongst other factors, on how the system duplexes received and transmitted signals. If it uses time division duplexing (TDD), the channel is alternately used by the base station and the mobile. If it uses frequency division duplexing (FDD), the channel is exclusively used by the base station.

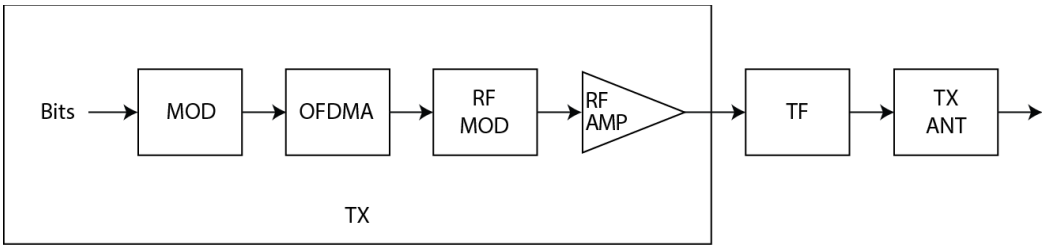

Figure 8. Block diagram of a BRS base station transmitter. MOD represents the baseband modulator, OFDMA represents the orthogonal frequency division multiple access operation, RF MOD represents the RF modulator, RF AMP represents the RF amplifier, TF represents the transmitter filter, and TX ANT represents the transmitter antenna.

3.5 Radar Target

We use the targets in the IEC 62388 standard clutter free tests [16],[21]when it is necessary to know all the target's characteristics such as range, height above water, and RCS. The set of targets is diverse in that it includes distributed targets such as shorelines, complex targets such as ships and boats, and point targets such as channel markers and buoys.

A summary of target parameters is provided in Table 1. The incongruity between the descriptive shoreline height and the height used in calculations is assumed to be due to terrain irregularity. Figure 9 displays the targets with respect to their RCS and range. Range limits for each pulse

width based on manufacturer literature are also shown. The short pulse is limited to ranges up to 5.6 km (3 nmi) and the long pulse from 5.6 to 44.4 km (3 to 24 nmi). The medium pulse range from 1.4 to 22.2 km (0.75 to 12 nmi) overlaps short and long pulse ranges.

Table 1. IEC 62388 standard clutter free test cases.

Case	Target	Height (m)	Range		RCS (m^2)
			nmi	km	
1	60m high shoreline	50.0	20.0	37.0	50000.0
2	6 m high shoreline	5.0	8.0	14.8	5000.0
3	3 m high shoreline	2.5	6.0	11.1	2500.0
4	SOLAS ship > 5000gt	10.0	11.0	20.4	30000.0
5	SOLAS ship > 500gt	5.0	8.0	14.8	1000.0
6	Small boat with reflector	4.0	3.7	6.8	0.5
7	Buoy with reflector	3.5	3.6	6.7	1.0
8	Buoy	3.5	3.0	5.6	0.5
9	Small 10 m long boat	2.0	3.0	5.6	1.4
10	Channel marker	1.0	1.0	1.9	0.1

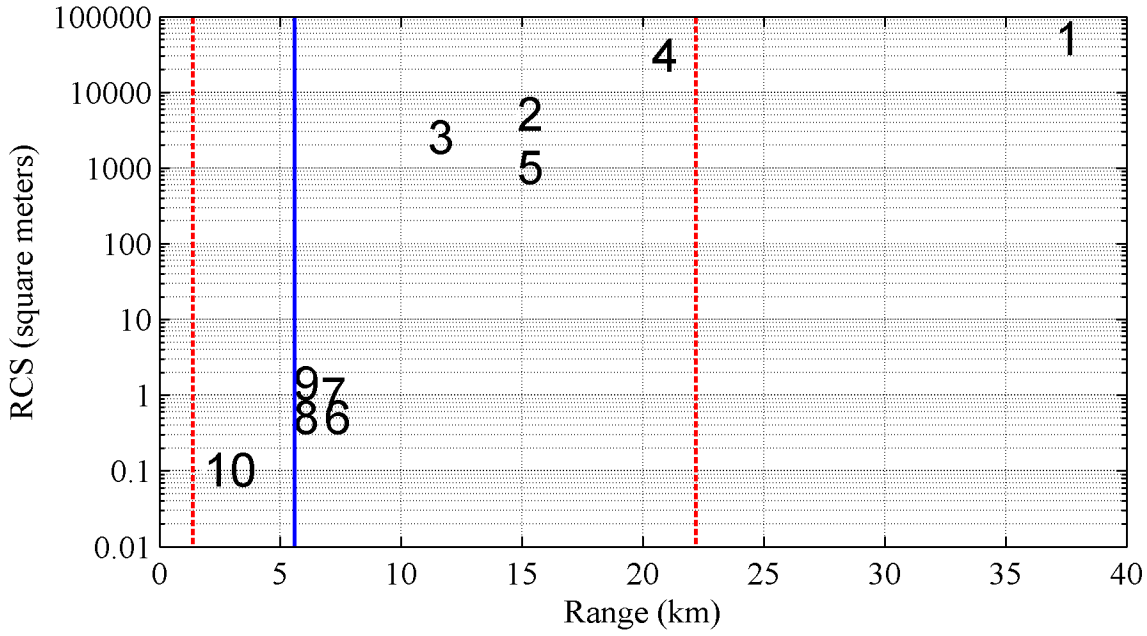

Figure 9. RCS and range for ten IEC 62388 standard clutter free test cases with pulse range limits. Short and long pulse ranges are separated by solid blue line at 5.6 km. Medium pulse ranges are between dashed red lines at 1.4 and 22.2 km.

3.6 Radio Wave Propagation Path Loss

Generally speaking, propagation path loss varies with location and time. Path loss varies over location because of differences in terrain and over time because of changes in atmospheric conditions such as rain, fog, or snow. However, in the maritime environment, terrain irregularity is minimal. Consequently, most variability is due to atmospheric conditions which change from hour to hour.

Path loss variability increases with path length. Short paths have lower and more constant path loss. Signals transmitted across short paths have higher powers and less power variability. Longer paths have higher and more variable path loss. Signals transmitted across long paths have lower powers and more variability.

In some cases atmospheric conditions can trap radio waves in atmospheric layers which create propagation ducts. Propagation ducts can decrease propagation path loss considerably as compared to free space. In the U.S., propagation ducts occur less than 10% of the time. The higher percentages occur in the south where there is significant variation from season to season [22].

4 MODELS

In this section we describe the various models used for interference analysis. Specific model parameter values are provided in Appendix A.

4.1 Radar System

The radar system model and its associated parameters are shown in Figure 10. The radar transmit power is p_{tx}. The impulse response of the radar transmitter filter is $h_t(t)$. The radar signal is modeled as a continuous wave modulated by a periodic, rectangular pulse. The pulse width, pulse repetition interval (PRI), and pulse repetition frequency (PRF) are τ, T, and f_p, respectively.

The transmitter and receiver share the same antenna whose gain is g. The propagation path loss from the radar to the target and from the target to the radar is l_p. Consequently the total path loss is l_p^2. The target RCS is σ.

The Gaussian noise block represents the composite receiver noise factor, f_{rx}. The receiver front-end gain and impulse responses are $g_{fe}$and $h_{fe}(t)$, respectively. The IF gain and impulse response are g_{if} and $h_{if}(t)$, respectively.

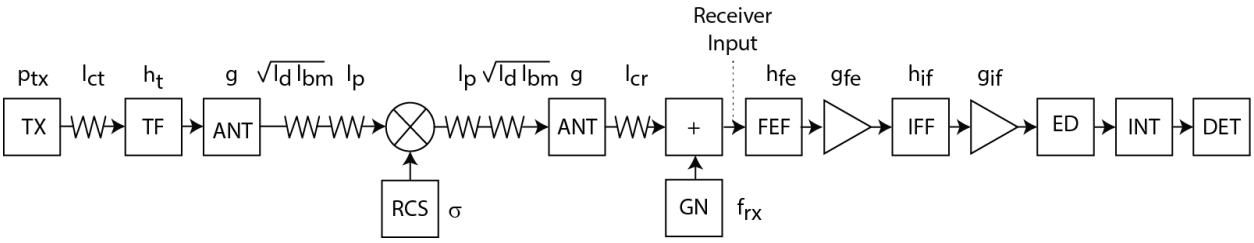

Figure 10. Radar system model. TX represents the transmitter source, TF represents the transmitter filter, ANT represents the antenna, RCS represents the radar cross section, FEF represents the front-end filter, GN represents Gaussian noise, IFF represents the IF filter, ED represents the envelope detector, INT represents the non-coherent integrator, and DET represents the threshold detector.

A number of losses, shown in Table 2, are common in these types of radars. The radome, which protects the antenna from weather, attenuates the radio wave during transmission and reception. The rotary joint, transmission line, and circulator introduce circuit losses. Integration beam shape loss is caused by the rotating antenna modulating pulse amplitude within the pulse integration period.

Finally, there are a number of losses associated with signal processing such as the IF filter not being matched to the transmitted pulse shape, the digitizer missing the highest signal, and the CFAR function misestimating the detection threshold.

Table 2. Radar losses.

Loss	Parameter	Equation	Notes
Transmitter circuit	l_{ct}		Circulator, transmission line, and rotary joint
Receiver circuit	l_{cr}		Rotary joint, transmission line, and circulator
Radome	l_d		Transmission and reception
Integration beam shape	l_{bm}		Transmission and reception
Signal processing	l_{sp}		
System	l_s	$l_{ct}l_{cr}l_d l_{bm}l_{sp}$	

Radar signal processors integrate pulses to enhance SNR. The number of pulses integrated within the time the rotating antenna beam is pointed at the target is determined from

$$n_p = \frac{\theta f_p}{6\omega_r} \tag{2}$$

where θ is the antenna 3 dB azimuth beam width in degrees, f_p is the PRF in Hz, and ω_r is the antenna rotation rate in revolutions per minute (RPM), assuming the antenna rotates completely around.

4.2 BRS System

The BRS system model, shown in Figure 11, is composed of the base station transmitter, circuit loss, transmitter filter, and antenna blocks. The transmitter contains the modulator, OFDMA block, RF modulator, and RF amplifier described previously. The transmitter filter decreases the unwanted emissions power. The power at the output of the transmitter source is $\hat{p}_{tx}$, the circuit loss from the transmitter block to the antenna is $\hat{l}_{ct}$, and the transmit antenna gain is $\hat{g}_t$.

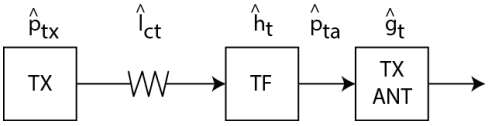

Figure 11. BRS model. TX represents the base station transmitter source, TF represents the transmitter filter, and TX ANT represents the transmitter antenna.

4.3 Radar Target

Radar targets are characterized by their RCS. In our analysis we assume that scattering off the target causes RCS fluctuations about a mean and the mean is dependent on target aspect angle, shape, and material. Aspect angle is the angle between the target longitudinal axis and the radar beam axis. The fluctuations are characterized by the exponential distribution probability density function

$$p(\sigma) = \frac{1}{\sigma_{av}} exp\left(-\frac{\sigma}{\sigma_{av}}\right) \tag{3}$$

where σ is the radar cross section and σ_{av} is the average or mean radar cross section. The exponential distribution is identical to that used in the Swerling 1 RCS model [23]. As in the Swerling 1 RCS model, fluctuations are assumed to be constant during the pulse integration period.

This model is inspired by ship RCS measurements [24] performed at 2.8 GHz with a horizontally polarized antenna in 2 degree azimuth increments. The RCS exceeded by 80, 50 (median), and 20 percent of all RCS measured at each azimuth are shown in Figure 12. Differences between the 20th and 80th percentiles are independent of aspect. However, the 50 percentile or median varies significantly. For example the median RCS is as high as 65 dBsm near 270 degrees aspect and as low as 40 dBsm near 0 degrees for a total 25 dB variation. Another study [25] found ship median RCS to vary on the order of 15 dB as the aspect changed from bow to broadside. Assuming the RCS is exponentially distributed, the median is approximately ln 2, 0.69, or -1.6 dB of the mean.

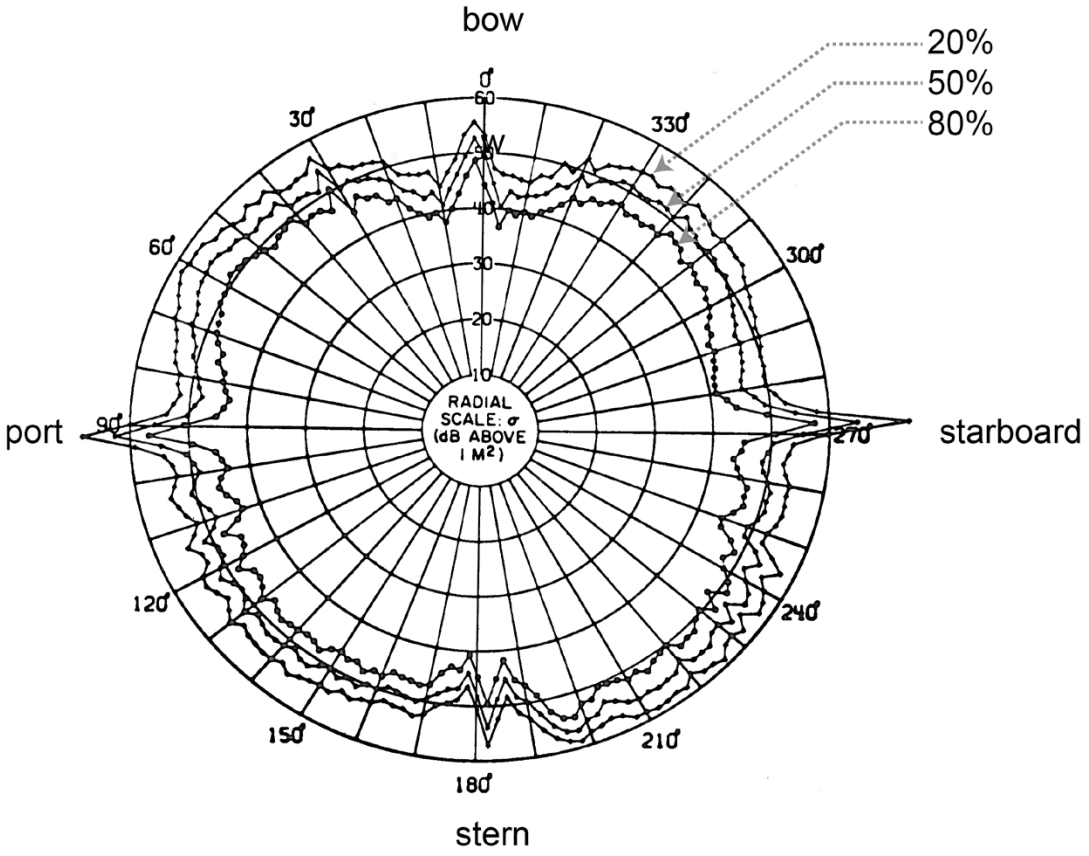

Figure 12. RCS patterns of a large naval auxiliary ship measured at 2.8 GHz with a horizontally polarized antenna in 2 degree azimuth increments. Traces from the center to outside represent values of RCS that are exceeded by 80, 50 (median), and 20 percent of all RCS measured at that azimuth. Bow and stern are at 0 and 180 degrees azimuth, respectively. (Figure adapted from Figure 2.21(a) in Merrill L. Skolnik, *Introduction to Radar Systems,* New York: McGraw Hill Book Company, 1980, p. 45.)

4.4 Radio Wave Propagation

The radar link, BRS link, and interference link between the two systems have radio wave propagation path loss which can vary with location and time. Characteristics of a number of propagation path loss models are discussed in Appendix B. The ITS Irregular Terrain Model (ITM) is used because our work needs both signal fading and enhancement statistics. Details regarding how ITM generates these statistics are provided in Appendix C.

Figures 13 and 14 show ITM hourly path loss statistics for the interfering signal path when the BRS antenna height is 30 meters, the ship radar height is 15 meters, and there is no precipitation. The results do not go below the model's 1 km minimum distance.

Path loss variability is evident from the spread of probabilities at a distance. The figures show that there is little path loss variability below 5 km. Path loss variability increases above 5 km and increases even more above 29 km, well before the 38 km smooth earth radio horizon where diffraction effects dominate.

The same scenario was evaluated for propagation over land. Because of the relatively low antenna heights compared to the separation distance and corresponding low grazing angle, over-land results were essentially the same as over-sea. Consequently, results over sea can be extended to mixed land sea paths where a portion of the path is over land.

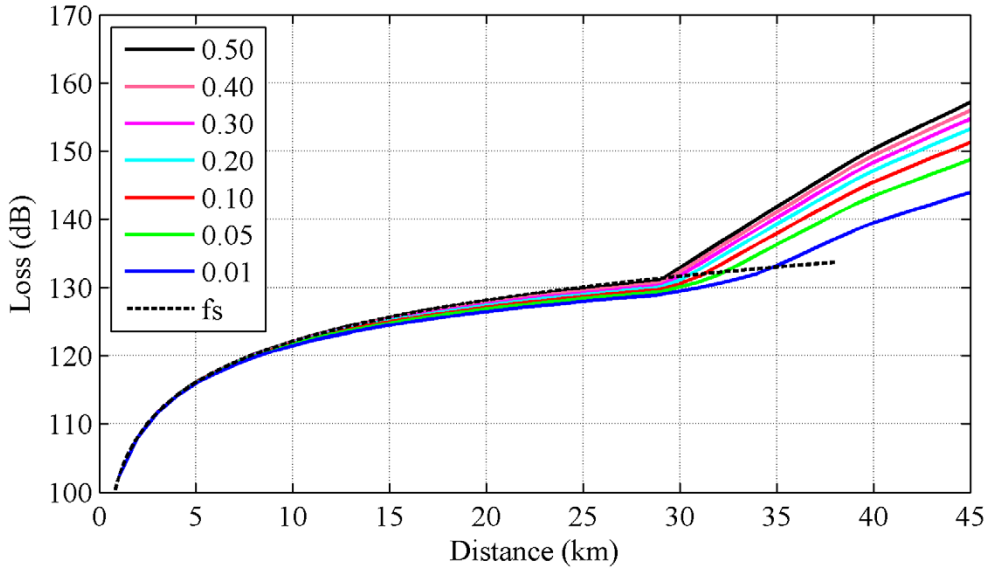

Figure 13. Probability loss is less than ordinate over a 45 km range.

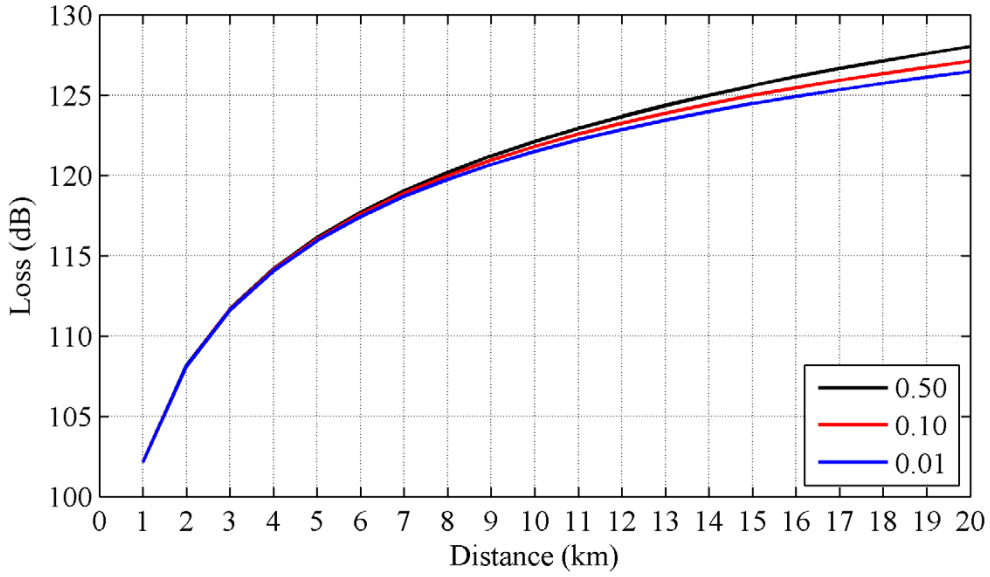

Figure 14. Probability loss is less than ordinate over a 20 km range.

4.5 Interference

The overall interference model is a combination of the radar, BRS, target, and radio wave propagation models as shown in Figure 15. The summation of multiple BRS signals represents the aggregate effect where the radar receives power from more than one base station. The significance of this effect is discussed in Section 6 .Two new parameters are introduced in this diagram. They are the propagation loss from the base station to the radar, $\tilde{l}_p$, and the antenna polarization loss between the base station and radar antennas, l_{pol}.

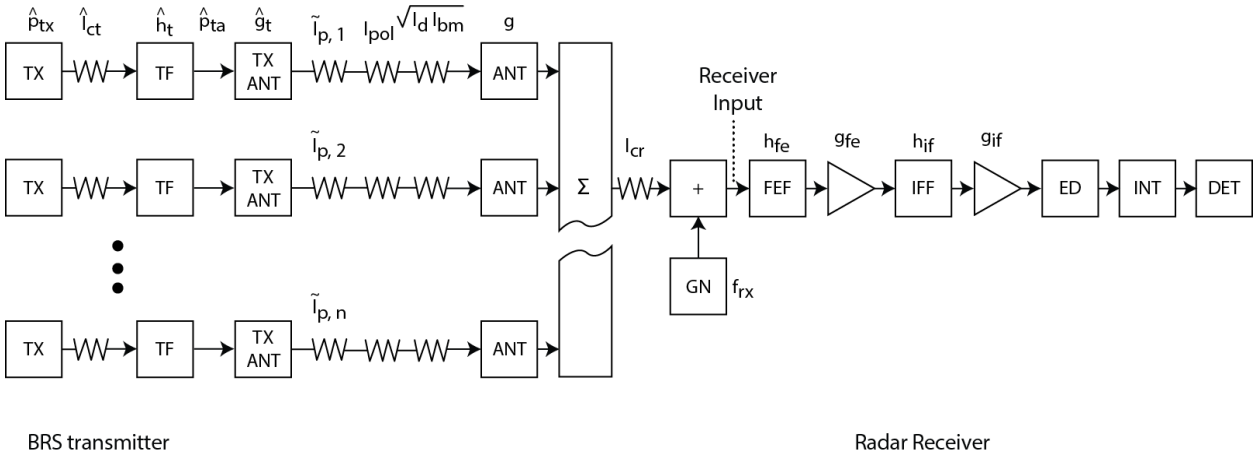

Figure 15. Interference model. TX represents the transmitter, TF represents the transmitter filter, TX ANT represents the transmitter antenna, ANT represents the radar antenna, GN represents Gaussian noise, FEF represents the front-end filter, IFF represents the IF filter, ED represents the envelope detector, INT represents the integrator, and DET represents the threshold detector.

5 BRS SIGNAL MODELLING

In interference analysis, it is often convenient to replace the actual signal with one that is more analytically tractable [26], [27]. In this case we would like to replace the signal transmitted from a BRS base station with Gaussian noise. This section shows measurements and statistical analysis that support this replacement.

The BRS base station signal we investigated conformed to the WiMAX OFDMA, time division duplexed (TDD) standard [28]. Since we are able to analytically separate on- and off-times we are assuming results for on-times would apply to frequency division duplexed (FDD) signals.

The signal was transmitted at a 2683.5 MHz center frequency and had an approximate 9.3 MHz equivalent noise bandwidth. The TDD on-time and period are 3 and 5 ms, respectively, which results in a 60% duty cycle. A single WiMAX OFDMA symbol with guard time is approximately 103 μs. In one 3 ms on-time there are approximately 29 OFDMA symbols.

5.1 Measurement System Description

The measurements were performed in a laboratory with the setup shown in Figure 16. The base station (BS) was connected to the user equipment (UE) by a cable. An attenuator in the cable replicated radio wave propagation path loss. The measurement system was connected to the cable with a directional coupler located between the path loss attenuator and the UE. The measurement system consisted of a custom preselector unit,[2] instrument, and computer. The instrument is either a spectrum analyzer (SA) or vector signal analyzer (VSA). The custom preselector unit had a variable attenuator, preselector filter, and low-noise amplifier (LNA).

The WiMAX spectrum was measured with the spectrum analyzer (SA). The WiMAX time series, used to analyze the signal statistics of smaller portions of the WiMAX spectrum, was measured with the vector signal analyzer (VSA). For the purposes of this section, the SA powers are reported as the power at the input to the preselector and the VSA powers are reported as the power at the input to the VSA.

The preselector filter had a 30 MHz bandwidth and approximately 8 dB loss at 3 GHz. The LNA had 25 dB gain and an approximately 4.5 dB noise figure at 3 GHz. SA and VSA noise figures were approximately 21 dB at 3 GHz. Measurement system noise figure was 15.2 dB at 3 GHz with the preselector.

[2] 3rd generation Radio Spectrum Measurement System (RSMS) preselector unit.

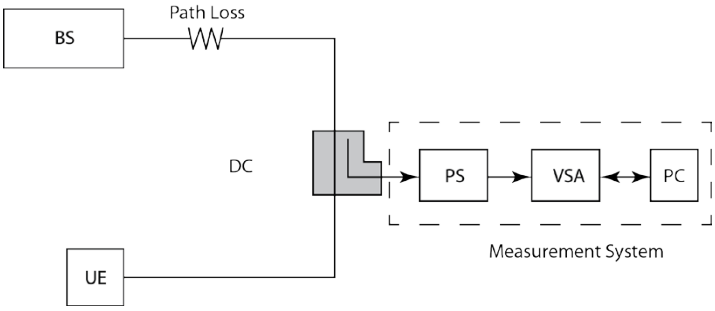

Figure 16. Measurement setup shown with VSA. BS represents the base station, UE represents the user equipment, DC represents the directional coupler, PS represents the preselector, and PC represents the personal computer.

5.2 WiMAX Spectrum

The WiMAX spectrum was measured with the stepped frequency measurement algorithm which maximizes measurement dynamic range by allowing the user to vary preselector attenuation as the measurement system center frequency is stepped across a range of frequencies. At frequencies where strong signals are present, attenuation is added. Conversely, at frequencies where weak signals are present, attenuation is reduced.

The average power of a signal with noise characteristics is best measured with an RMS voltage or average power detector. Since a spectrum analyzer with average power detection was unavailable, average power detection was approximated by envelope detection followed by 10 Hz video bandwidth filtering, 0.5 second per step integration time, sample detection, and addition of a 2.5 dB noise correction factor to the measured power.

Figure 17 shows the noise corrected PSD measurement in terms of power at the preselector input. The measurement was performed with a 1 MHz frequency step and 100 kHz resolution bandwidth. The center frequency and bandwidth are estimated to be 2683.5 MHz and 9.3 MHz, respectively. A horizontal line at -108.8 dBm demarks the average measurement system noise power, often referred to as the noise floor.

The signal is occupying a 10 MHz BRS channel adjacent to the lower edge of the 2700–2900 radar band and has unwanted emissions above and below the BRS channel. The unwanted emissions below the BRS channel fall to approximately -90 dBm by 2640 MHz then level off until 2450 MHz where they reach the measurement system noise floor. Unwanted emissions above the BRS channel fall to the noise floor by 2760 MHz.

Unwanted emissions are precisely defined by the ITU-R [29], which recognizes three transmitted signal power spectral density (PSD) domains referred to as necessary bandwidth, out-of-band (OOB), and spurious. Collectively, OOB and spurious emissions are referred to as unwanted emissions. The necessary bandwidth contains most of the modulated signal power, the spurious region contains unwanted signals incidental to transmission, and the OOB region between them contains both modulated and incidental signals.

In general the OOB domain begins at the edge of the necessary bandwidth and ends at ± 2.5 times the necessary bandwidth from the transmitter center frequency. The spurious domain follows the OOB domain. The boundaries of these domains can be adjusted to meet various spectrum management objectives. For example the ETSI UMTS standard [12] has different power limits for spurious emissions in the BRS band and spurious emissions outside of the BRS band.

Using ITU-R definitions, the necessary bandwidth is 10 MHz and within 2678.5 to 2688.5 MHz, the out-of-band emissions extend from 2658.5 to 2678.5 MHz and 2688.5 to 2708.5 MHz. The spurious emissions extend below 2658.5 MHz and above 2708.5 MHz.

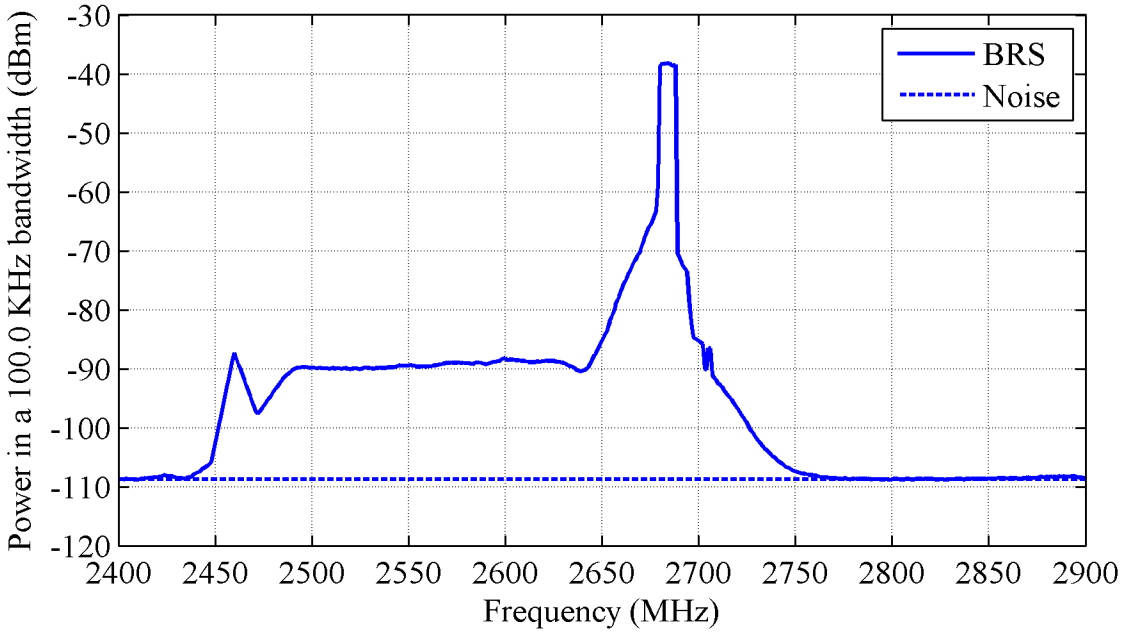

Figure 17. PSD measurement. (Data Identifier: F6R2)

5.3 Signal Statistics Measurements

Signal statistics measurements were made at 2550, 2683.5, and 2750 MHz with the VSA. The 2683.5 MHz measurement is made at the BRS signal center frequency and represents the signal in the necessary bandwidth. The 2550 MHz measurement is made where unwanted emissions are not attenuated by a transmitter filter. It is representative of spurious emissions inside the BRS band. The 2750 MHz measurement is made where unwanted emissions are attenuated by the transmitter filter. It is representative of filtered spurious emissions outside the BRS band.

The measurement in the necessary bandwidth was taken without the preselector. The remaining spurious measurements used the preselector to reject the strongest portion of the signal in the necessary bandwidth and thereby increase measurement dynamic range.

The VSA converts the real passband signal at a center frequency to a complex baseband (i.e. inphase and quadrature) signal centered at 0 Hz. The measurements were made in an 18 MHz VSA two-sided bandwidth. The signal was sampled at 23.041 MHz with a time increment of 43.4 ns.

VSA input range varied with the center frequency as shown in Table 3. The VSA begins compressing a CW signal at approximately 8 dB above the input range [30]. Caution should be used when commenting on measurements with samples that are more than 8 dB above the input range.

Table 3. Measurement system parameters. The measurement center frequency f_{meas} varies. The BRS center frequency, f_{brs}, is 2683.5 MHz.

f_{meas} (MHz)	$f_{meas} - f_{brs}$ (MHz)	VSA input range (dBm)	Preselector attenuation (dB)	Description
2550.0	-133.5	-30	0	Spurious domain inside BRS band
2683.5	0	0	NA	Necessary bandwidth
2750.0	66.5	-45	0	Spurious domain outside BRS band

5.3.1 Analysis Details

Statistical analysis consisted of calculating the signals amplitude probability distribution (APD) and power spectral density (PSD). The APDs were plotted on Rayleigh graphs where the Rayleigh distributed amplitude of complex baseband Gaussian noise appears as a straight, negatively sloped line with mean power at approximately the 37th percentile. The PSD of white Gaussian noise (WGN) is flat; colored Gaussian noise may be any shape but flat. Measurement system noise is represented by the dashed red line on these graphs.

The periodicity of TDD causes the signal statistics to be cyclostationary. We addressed this issue by separating the signal into distinct on- and off-time signals which we analyzed as though they were stationary. It is important to note that incidental unwanted emissions and measurement system noise are present at all times. The on- and off-time signals were obtained by multiplying the data by a gating function specified by an on-time, period, and delay and removing residual zeros.

Processing used 4,194,304 or 2^{22} samples which were separated into 2,516,582 on-time samples and 1,677,721 off-time samples. The samples spanned 182 ms or 36.4 TDD periods. For APD processing the samples were decimated by 3 to assure sample independence yielding approximately 838,860 on-time samples and 559,240 off-time samples. For PSD processing 524,288 un-decimated on- and off-time samples organized into 512 blocks of 1024 samples were used. The corresponding block period was 44.4 μs which produced a 22,500 Hz frequency resolution.

5.3.2 2683.5 MHz

The 2683.5 MHz signal represents the signal in the necessary bandwidth. Figure 18 shows a sequence of TDD frames with prominent on- and off-times. The on-time has a dip in amplitude that begins and ends at approximately 100 and 300 μs, respectively. This feature is caused by lower power preamble and control information OFDMA symbols. Data OFDMA symbols fill the rest of the on-time.

Figures 19 and 20 are the APD and PSD of the whole signal over a number of TDD periods. The APD, broken into two segments, shows the differences in amplitudes between the on- and off-times. The break between the two occurs at the percent corresponding to the duty cycle. Although illustrative, this APD is not useful for determining whether the signals are Gaussian since it does not address the signal's statistical cyclostationarity. The PSD is flat and the bandwidth corresponds to the signal's.

Figures 21 and 22 are the APD and PSD of the signal after they have been separated into distinct on- and off- time signals. The gating function on-time, period, and delay parameters were 3000, 5000, and 2704 μs, respectively.

The on-time APD resembles GN with the exception of the flattening below 1 percent. This flattening could be due to OFDMA peak suppression. However since it occurs where VSA overload begins we cannot be entirely certain. The on-time PSD resembles WGN across the necessary bandwidth. The on-time power, 2.3 dBm, is greater than the whole signal's power, -0.2 dBm, by approximately the reciprocal of the duty cycle.

The off-time statistics are elevated above measurement system noise indicating that the off-time signal is due to incidental emissions from the transmitter and not the measurement system. The off-time APD resembles that of GN and the off-time PSD resembles that of WGN.

With the exception of the possible overload in the small on-time APD percentages, these statistics show that the on- and off-times can be reasonably emulated with WGN.

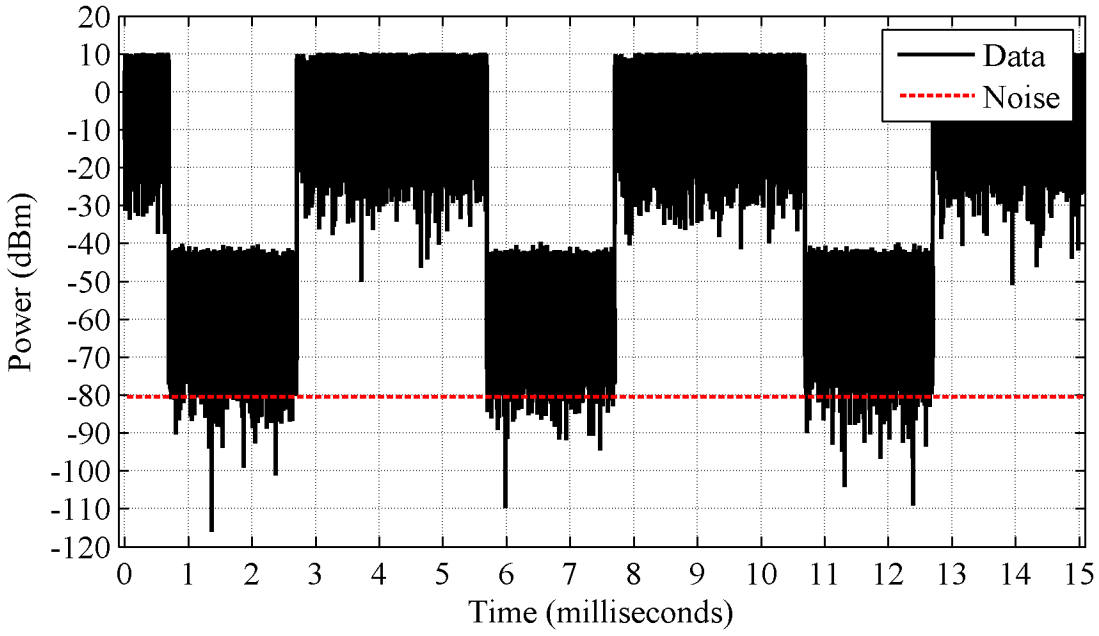

Figure 18. Signal at 2683.5 MHz showing TDD on- and off-times.

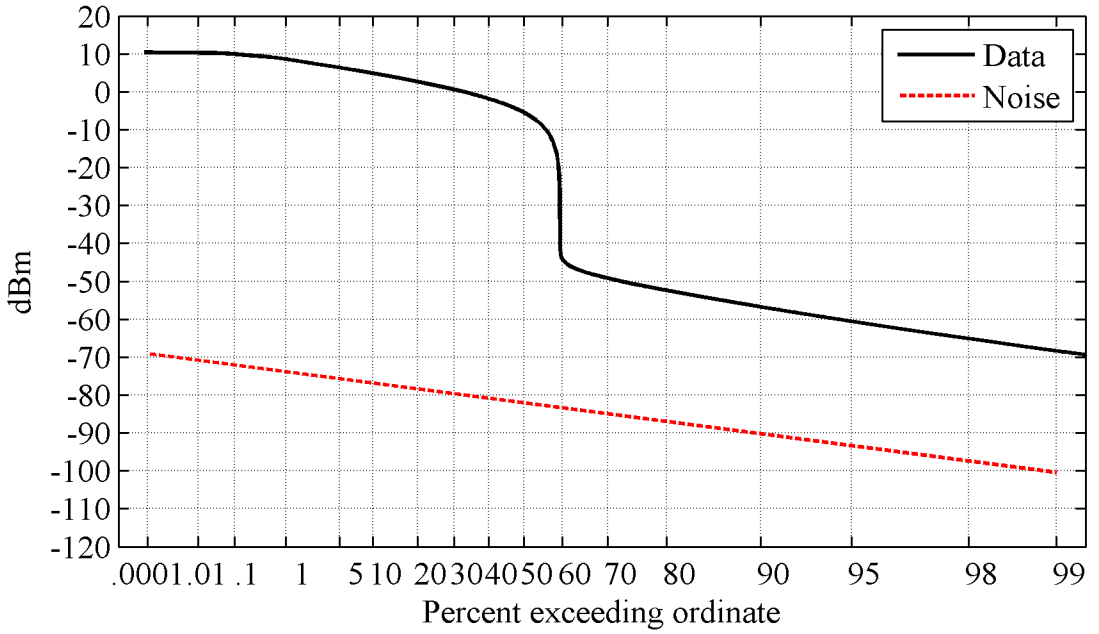

Figure 19. APD at 2683.5 MHz. On- and off-times have not been differentiated.

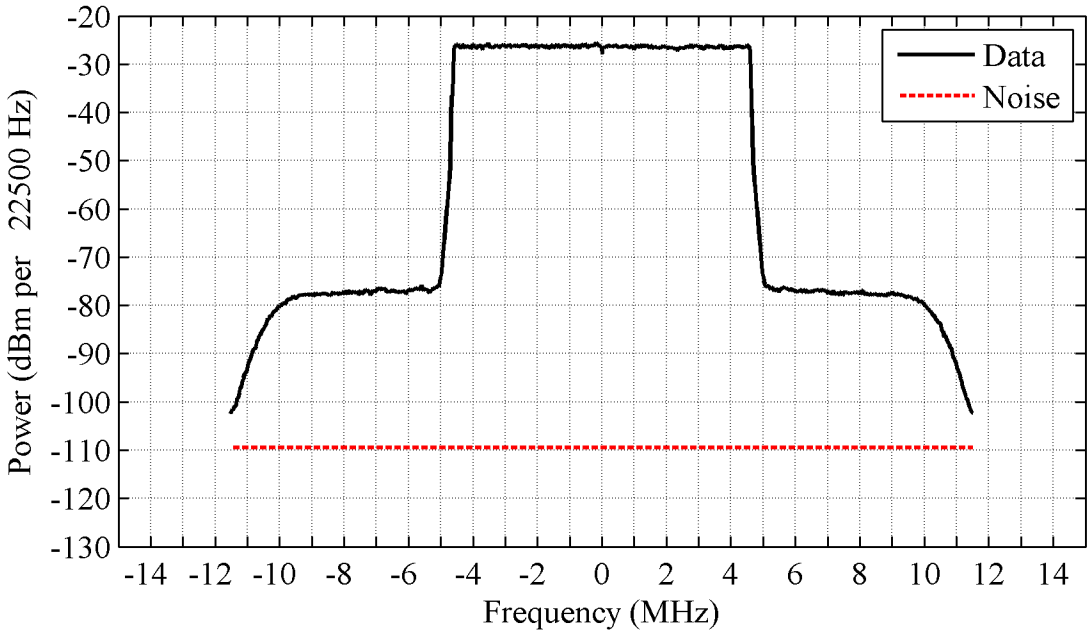

Figure 20. PSD at 2683.5 MHz. On- and off-times have not been differentiated.

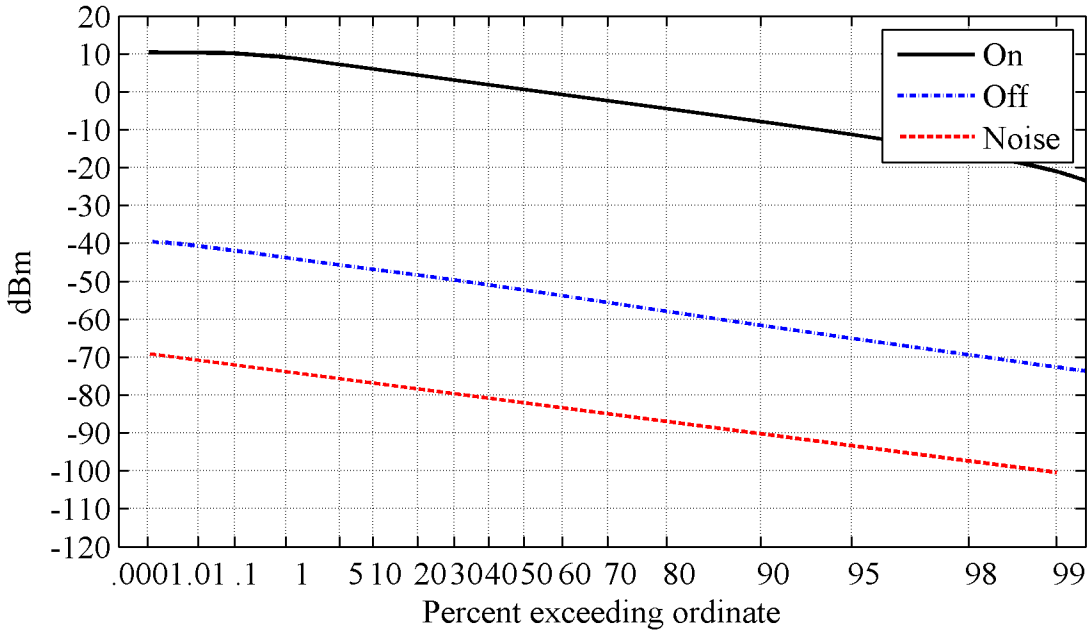

Figure 21. APD at 2683.5 MHz of on- and off-time signals.

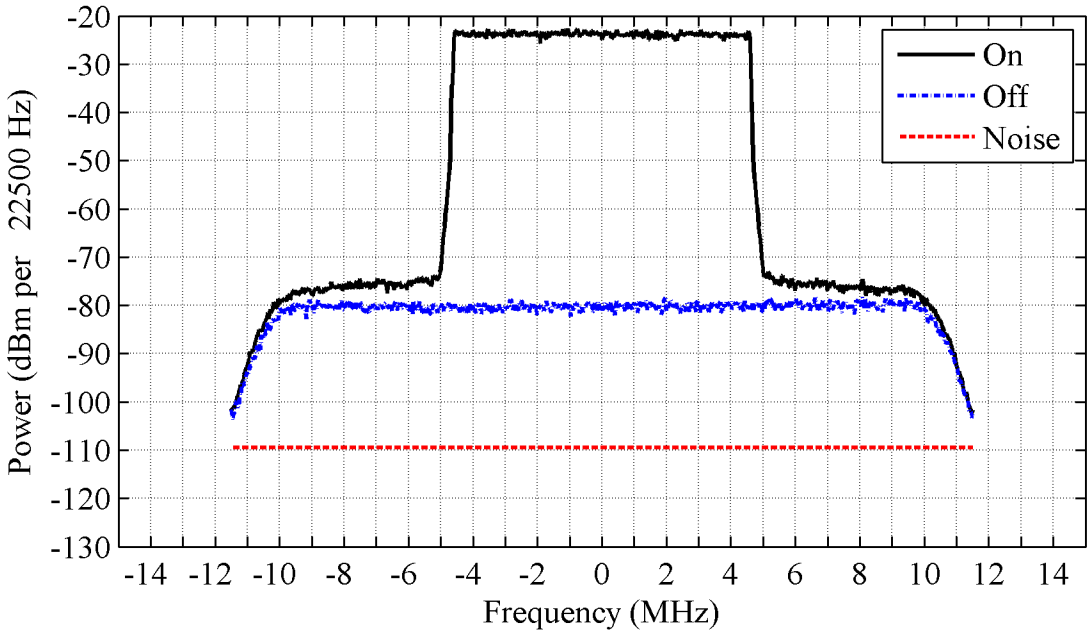

Figure 22. PSD at 2683.5 MHz of on- and off-time signals.

5.3.3 2550 MHz

The signal at 2550 MHz represents unwanted spurious emissions inside the BRS band. Figure 23 shows that the signal has well defined on- and off-times. Preamble and control OFDMA symbols are not evident at the beginning of the on-time. The gating function on-time, period, and delay parameters were 3018, 5000, and 2495 μs, respectively.

The on-time APD in Figure 24 resembles that of Gaussian noise and the on-time PSD in Figure 25 resembles that of WGN. The off-time APD also resembles Gaussian noise and the PSD resembles that of WGN. Both off-time statistics are approximately one dB above receiver noise indicating that the incidental emissions from the transmitter are approximately 6 dB below receiver noise.

The APD and PSD analysis indicates that on- and off-time emissions can be emulated by WGN.

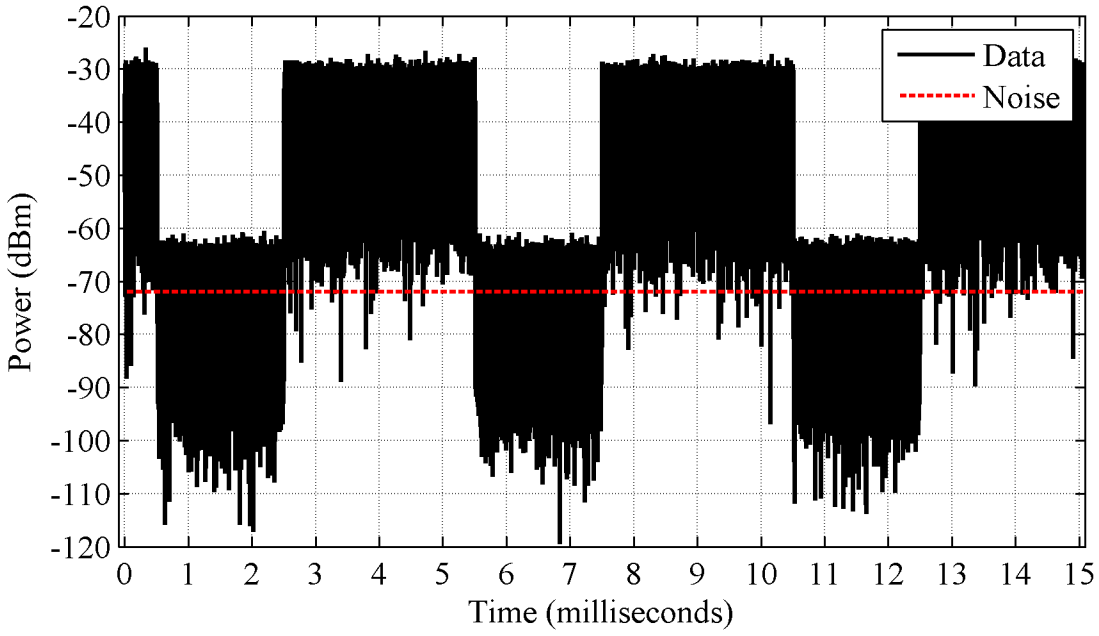

Figure 23. Signal at 2550 MHz showing TDD on- and off-times.

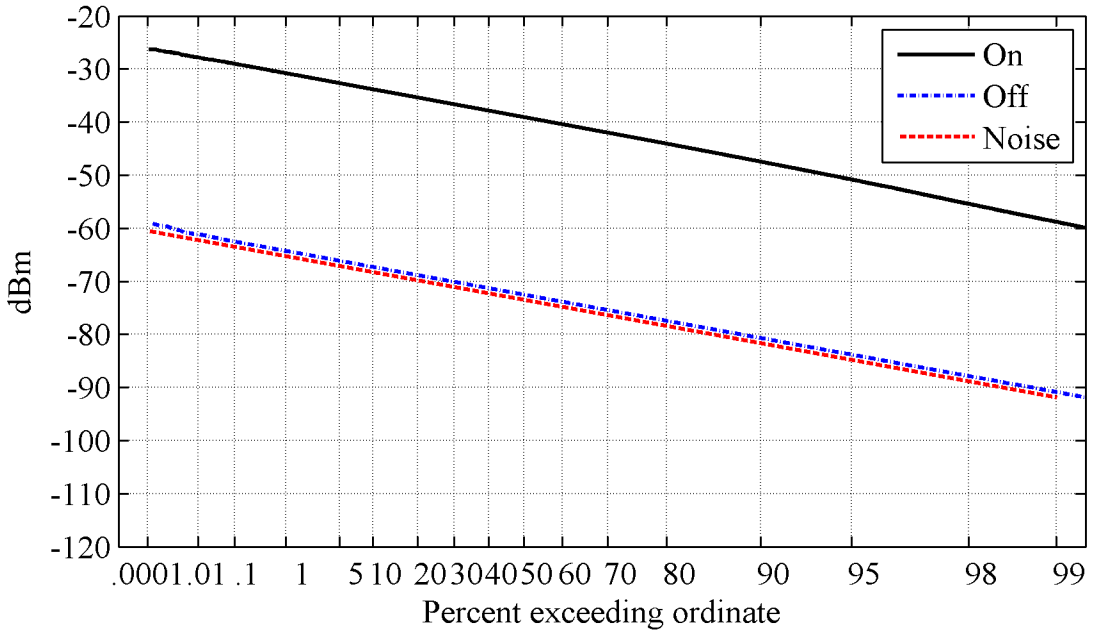

Figure 24.APD at 2550 MHz for on- and off-times.

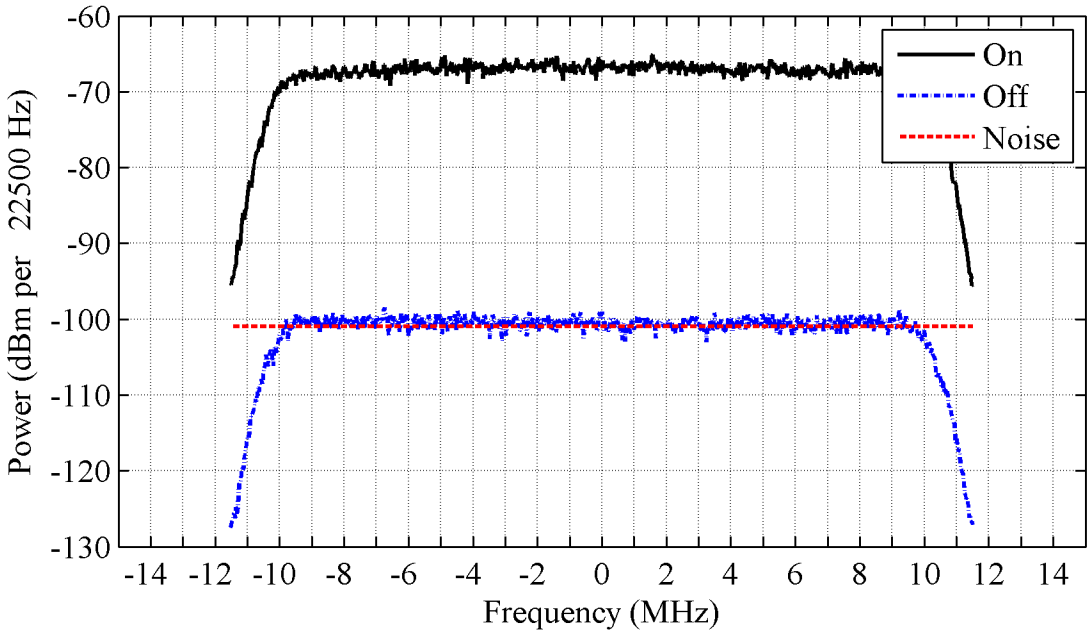

Figure 25.PSD at 2550 MHz for on- and off-times.

5.3.4 2750 MHz

The signal at 2750 MHz represents unwanted spurious emissions outside the BRS band. The emissions are at a lower power level after being attenuated by the transmitter filter. Figure 26 shows on- and off-times that are differentiated by an approximately 4 dB change in amplitude. There is no evidence of specific preamble or control word OFDMA symbols. The gating function on-time, period, and delay parameters were 3000, 5000, and 5135 μs, respectively.

The on-time APD in Figure 27 resembles that of Gaussian noise but the on-time PSD in Figure 28 has a definite slope from low to high frequencies, i.e. it is colored rather than white. The off-time APD resembles that of Gaussian noise and the off-time PSD resembles that of WGN.

The 2750 MHz measurement was reduced to a 1 MHz bandwidth signal centered at 2741 MHz or -9 MHz on the PSD graph to increase SNR. Results are consistent with the 2750 MHz measurement.

These analyses indicate that the on-time emissions can be emulated with colored GN and the off-time with WGN.

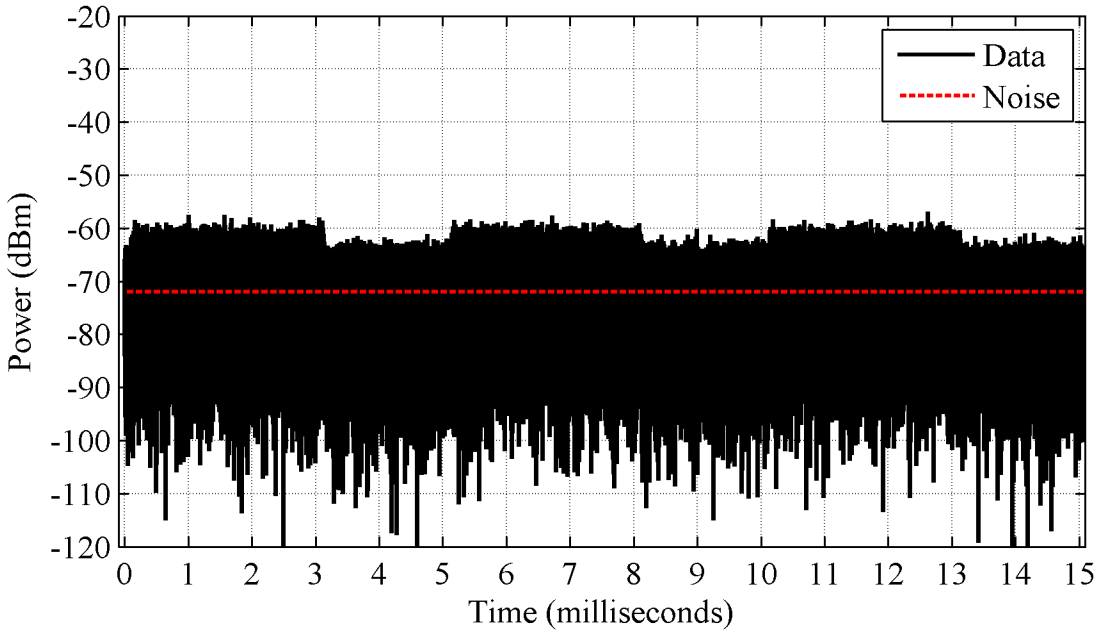

Figure 26. Signal at 2750 MHz showing TDD on- and off-times.

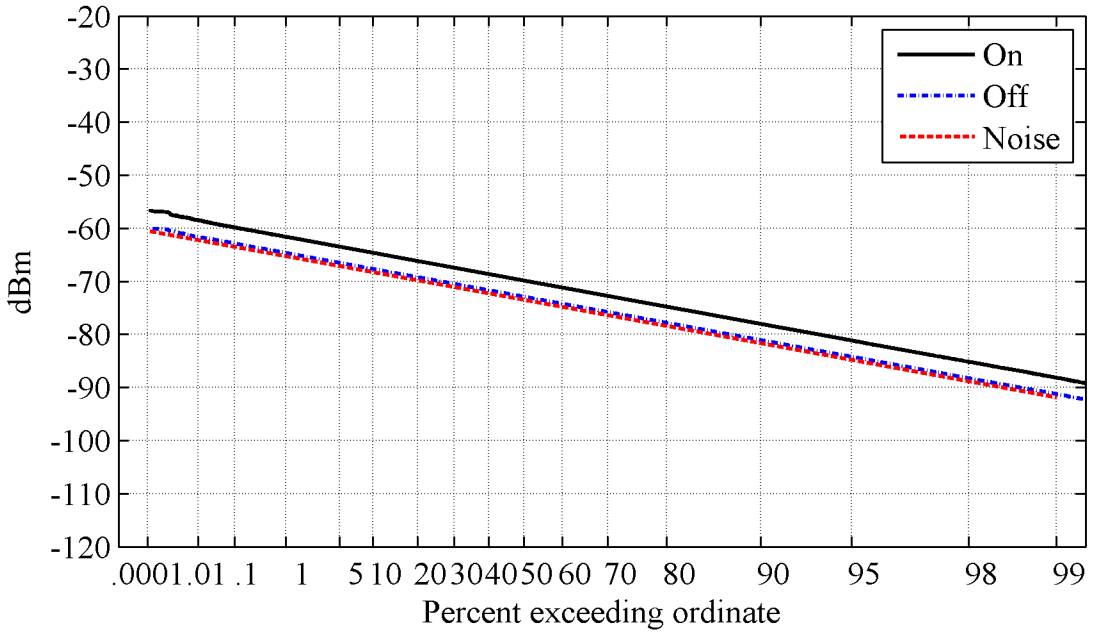

Figure 27. APD at 2750 MHz for on- and off-times.

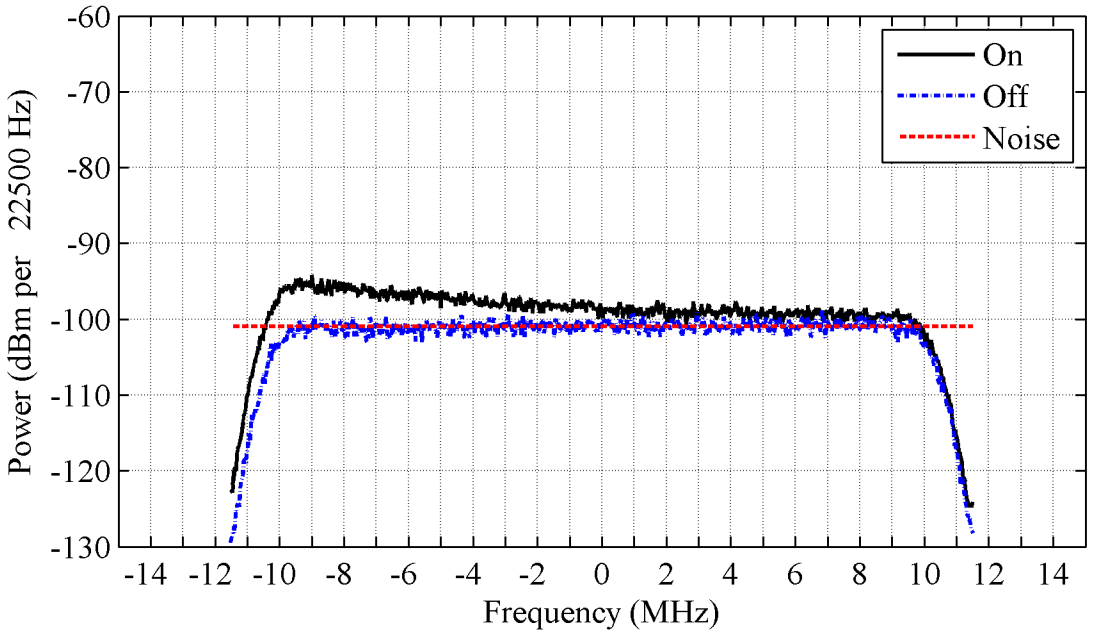

Figure 28. PSD at 2750 MHz for on- and off-times.

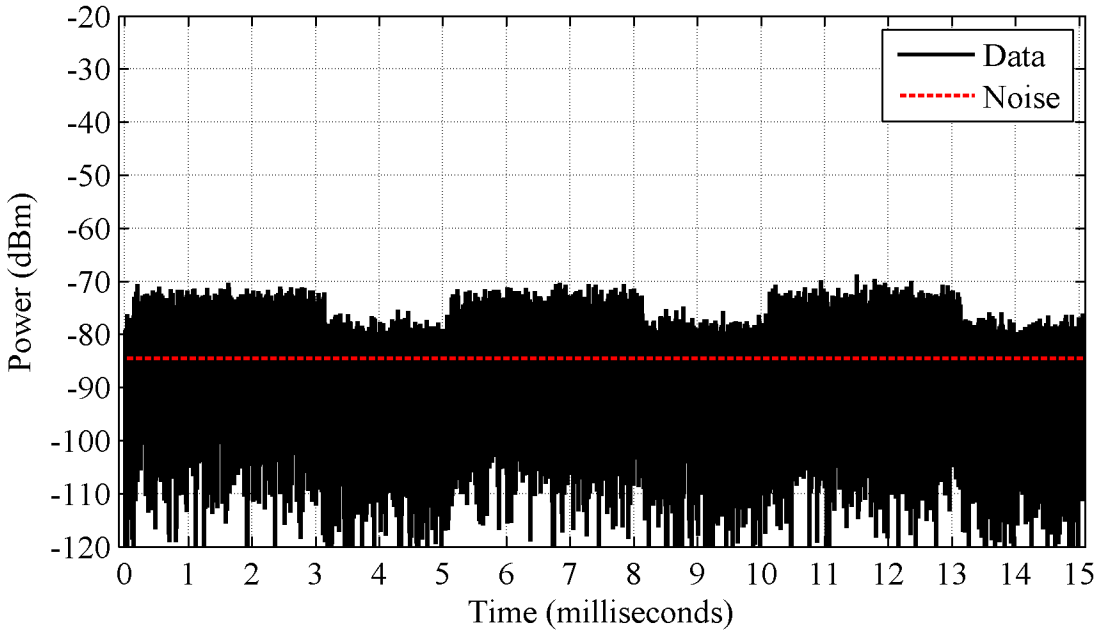

Figure 29. 2741 MHz, 1 MHz bandwidth signal derived from 2750 MHz measurement.

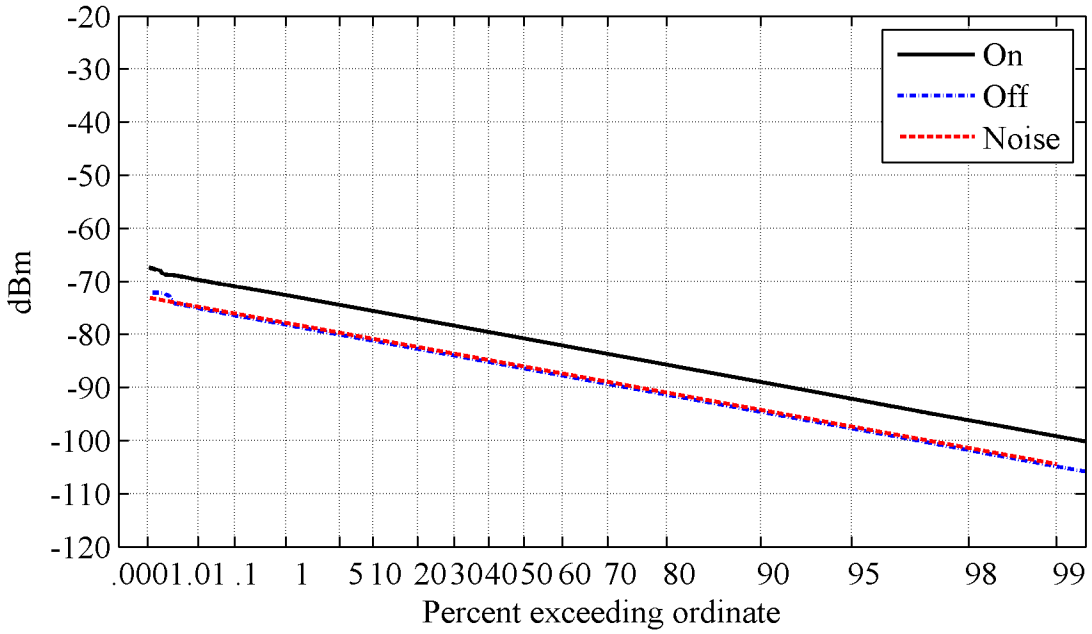

Figure 30. 2741 MHz, 1 MHz bandwidth APD derived from 2750 MHz measurement.

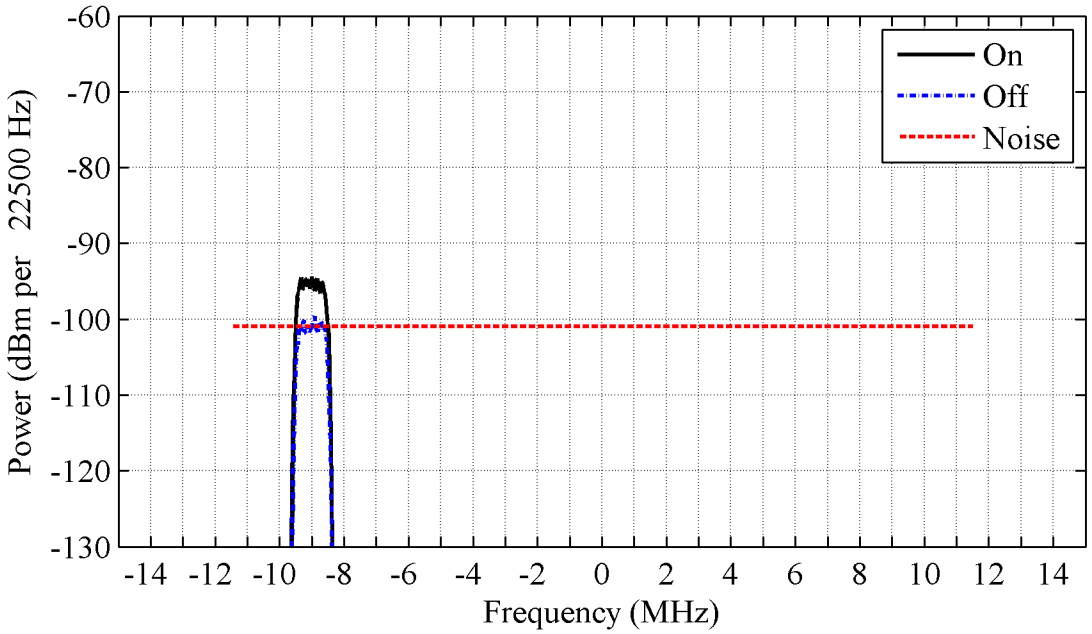

Figure 31. 2741 MHz, 1 MHz bandwidth PSD derived from 2750 MHz measurement.

5.4 Discussion

The results of our analysis are summarized in Table 4. The analysis showed that the 2683.5 MHz signal in the necessary bandwidth was approximately or nearly Gaussian. It is nearly Gaussian because on-time signal levels occurring less than 1% of the time were slightly compressed compared to GN. This could be due to OFDMA peak suppression but also may be due to VSA overload.

The analysis also showed that the 2550 MHz unfiltered spurious emissions below the BRS channel can be modeled as WGN during both on- and off-times. Finally, the analysis showed that the 2750 MHz filtered spurious emissions above the BRS channel have WGN characteristics during the off-time and colored GN characteristics during the on-time.

The roll-off or OOB regions between necessary bandwidth and the spurious regions were not measured due to measurement system dynamic range considerations. Pending future measurements, we will assume OOB emissions are Gaussian as well.

It is important to note that the noise outside of the necessary bandwidth can be colored and therefore correlated over time. The correlation decreases the number of independent samples but does not prevent us from using GN theoretical results in our analysis of BRS interference effects. Correlation is quantified by correlation time, which we assume to be short compared to the magnetron radar pulse repetition interval. Therefore correlation will not affect the integrated radar pulse statistics.

The analysis was done in a wide measurement bandwidth. However, since the statistics are Gaussian they will be Gaussian in smaller bandwidths as well. Consequently we can conclude that unwanted emissions from the BRS base station signals can also be modeled as GN processes for bandwidths smaller than our measurement bandwidth.

Finally, BRS base stations operate in a network and a victim receiver is likely to see emissions from an aggregate or number of base stations at once. Since the emissions from a single base station are Gaussian and the sum of any number of Gaussian random variables is still Gaussian it follows that the emissions from any number of base stations in an aggregate will also be Gaussian.

Table 4. Measurements' resemblance to Gaussian noise (GN) and white Gaussian noise (WGN).

f_{meas} (MHz)	On-time		Off-time		ITU Domain
	GN	WGN	GN	WGN	
2683.5	Nearly	Yes	Yes	Yes	Necessary bandwidth
2550.0	Yes	Yes	Yes	Yes	Spurious
2750.0	Yes	No	Yes	Yes	Spurious

6 AGGREGATE BRS SIGNAL POWER

In this section we are interested in determining how much greater the aggregate BRS signal power from all base stations in the network is than the power from a single BRS base station. If it is significantly more, interference analysis needs to be done with the aggregate BRS signal and its statistics.

6.1 Interference Power from a Single Base Station

The general interference link power budget for a single base station is

$$i_{single}(d) = \frac{\hat{p}_{ta}\,\hat{g}_t g}{\sqrt{l_d l_{bm}}\, l_{pol} l_{cr} \tilde{l}_p(d)} \tag{4}$$

where d is the distance from the radar to the base station, $\hat{p}_{ta}$ is the signal power at the transmit antenna, $\hat{g}_t$ is the gain of the base station antenna in the direction of the radar, g is the gain of the radar antenna in the direction of the base station, l_d is the radome loss, l_{bm} is the beam shape loss, l_{pol} is the polarization loss between the base station and radar antennas, l_{cr} is the radar receiver circuit loss, and $\tilde{l}_p$ is the path loss from the base station to the radar. Note that $\tilde{l}_p = \tilde{a}\tilde{l}_{fs}$ where $\tilde{a}$ is the excess path loss and $\tilde{l}_{fs}$ is free space path loss. In general, the interference power is a random variable due propagation path loss variability.

6.2 Effects of Narrow Radar Antenna Beam Width on Aggregate Power

We begin by assuming that the base stations coverage areas can be represented by tessellated hexagons as shown in Figure 32, where the dots in the hexagons represent base station locations. We also assume that the maximum aggregate power received by a narrow radar antenna beam width will come from base stations along a line of repetitively-spaced base stations.

There are only two such lines that connect repetitively-spaced base stations. The lines, labeled l_1 and l_2, connect base stations across the hexagonal sides and vertices, respectively, and terminate at ship locations labeled P_1 and P_2 , respectively. The ships are located distance d_1 from the base station at point B.

Using the hexagon parameters in Figure 33 it can be shown that the repetitively-spaced base station distances are AB=$\sqrt{3}t$ for line l_1 and EB=$3t$ for line l_2. Consequently the base stations along line l_1 are more closely spaced and a ship at point P_1 will receive more aggregate power than a ship at point P_2.

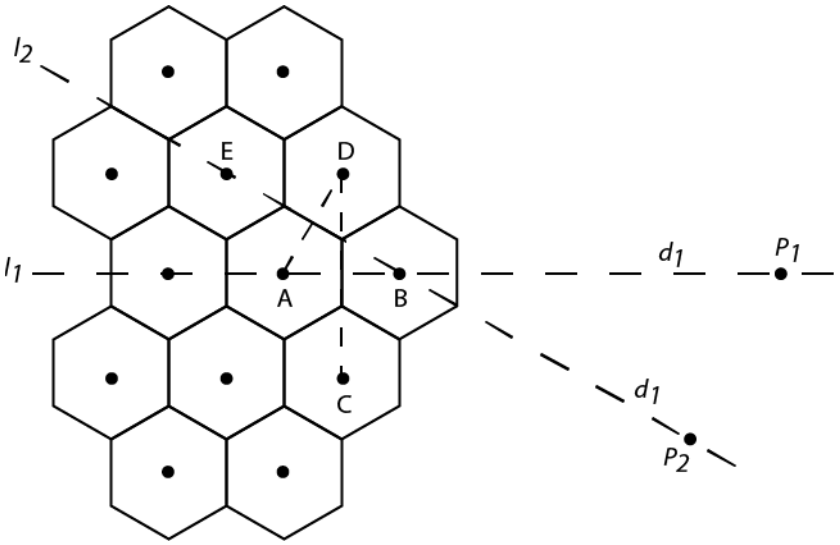

Figure 32. BRS coverage area composed of tessellated hexagons. Base stations are located at dots at center of hexagons. Ships are located at points P_1 and P_2.

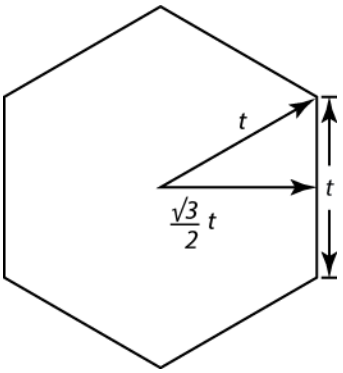

Figure 33. Relevant hexagon parameters.

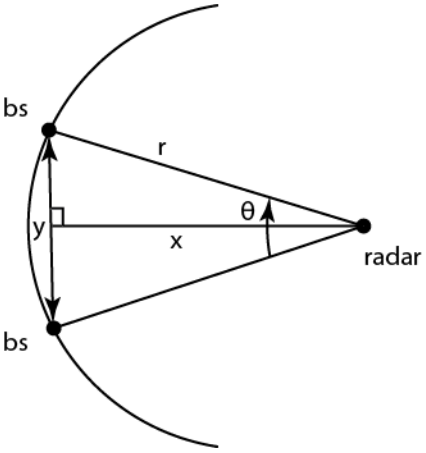

Figure 34. Chord length calculation parameters. Base stations are located at points labeled bs.

Next we calculate at what distance the radar antenna main beam will receive signals from base stations distances CD/2 and AD/2 from lines l_1 and l_2, respectively. We want to ensure the aggregate power can be adequately represented without including base stations near but not on the line. As shown in Figure 34, the two base stations define the chord, y, subtended by an angle corresponding to the antenna beam width, θ. The length of the chord is

$$y = 2r \sin(\theta/2), \tag{5}$$

the length of the radius is

$$r = \frac{y}{2 \sin(\theta/2)} \tag{6}$$

and the distance of interest is

$$x = \sqrt{r^2 - (y/2)^2}. \tag{7}$$

The chord AD for line l_2 is equal to $\sqrt{3}t$ and is the same as the distance between base stations which we assume to be 3.0 km. The chord CD for line l_1 is $3t$ or 5.2 km. Finally, assuming the antenna beam width, θ, is 1.9 degrees then x is 156.7 km for line l_1 and 90.4 km for line l_2. Calculations have shown little change in aggregate power past 10 base station distances or 30 km. Consequently, our aggregate model does not need to include base stations near the lines.

In summary, because of the radar antenna's narrow azimuthal beam width, maximum aggregate interference is from base stations along the line formed by the most closely repetitively-spaced base stations as shown in Figure 35.

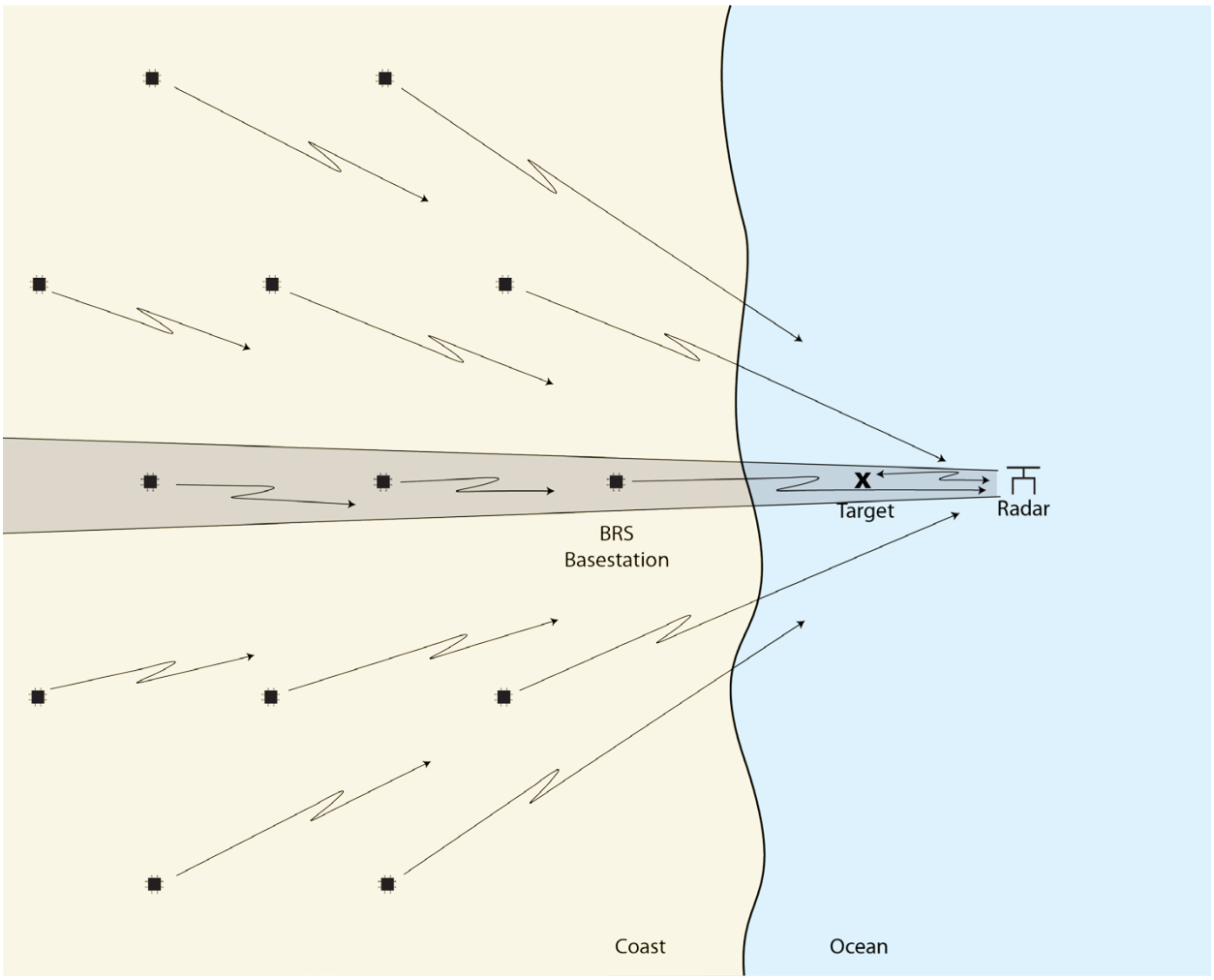

Figure 35. Interference scenario after taking into account narrow azimuthal beam width of the marine radar antenna. The base stations in the shaded area will provide the most interfering signal power.

6.3 Interference Power from a Set of Base Stations

The aggregate BRS signal power from base stations along the line formed by the most closely repetitively-spaced base stations is

$$i(d_1) = \sum_{n=1}^{N} i_{single}(d_n) = \sum_{n=1}^{N} \frac{\hat{p}_{ta}\,\hat{g}_t g}{\sqrt{l_d l_{bm}}\, l_{pol} l_{cr} \tilde{l}_p(d_n)} \tag{8}$$

where N is the number of base stations and n is the base station index. The aggregate separation distance, d_1, is defined as the distance from the radar to the closest base station along the line. The distance from the closest base station to the nth base station along the line is

$$d_n = d_1 + (n-1)d_{brs}, \quad n > 1 \tag{9}$$

where d_{brs} is the distance between adjacent base stations.

Because of propagation path loss variability, the aggregate power is a random variable with a statistical distribution. The aggregate power distribution is different than the power distribution of any one base station. Although the aggregate distribution mean is equal to the sum of the base station distribution means, this is not necessarily true for any other quantile. To find other quantiles the aggregate distribution must be determined.

The aggregate distribution can be computed using the ITM and Monte Carlo techniques. Specifically, the excess path loss means and pseudo-standard deviations of the individual interfering stations at distances $\{d_1, \ldots d_N\}$ are obtained from the ITM, and these are used along with the link budget to generate a random set of interfering powers, $\left\{i_{single}(d_1), \ldots i_{i_{single}}(d_N)\right\}$, which are added together to get $i(d_1)$. We then repeat this process M times, order the results, and pair them with corresponding probabilities $\left\{1, \frac{M-1}{M}, \cdots \frac{1}{M}\right\}$.

If the smallest interference power is paired with the smallest probability, $1/M$, we have the cumulative distribution function

$$F(i) = Pr\{i < i\}. \tag{10}$$

Similarly, if the smallest is paired with probability 1 we have the complementary cumulative distribution function

$$G(i) = Pr\{i \geq i\} = 1 - F(i). \tag{11}$$

The number of Monte Carlo trials determines how confident we can be in our results. This is particularly important at the lowest probabilities where there are fewer samples. We found that 10^6 trials is a reasonable number in predicting quantiles with probabilities as low as 1%. We also tested our random number generator for normality for sample sizes up to 10^7, with very satisfactory results. Consequently we are confident that we can predict quantiles with probabilities as low as 1% with 10 base stations in the aggregate.

6.4 Single Base Station and Aggregate Interference Power Statistics

Figure 36 shows various interference power quantiles from distributions across a range of distances from an aggregate of 10 base stations spaced 3 km apart. Parameters for the calculations are taken from Appendix A. As expected, power variation increases with distance. The figure also shows the difference between received interference power from an aggregate of 10 base stations and the interference power from a single base station. The difference is greatest between 5 and 30 km. At 15 km the difference is approximately 6 dB. Consequently, it is important to use the aggregate signal for interference analysis.

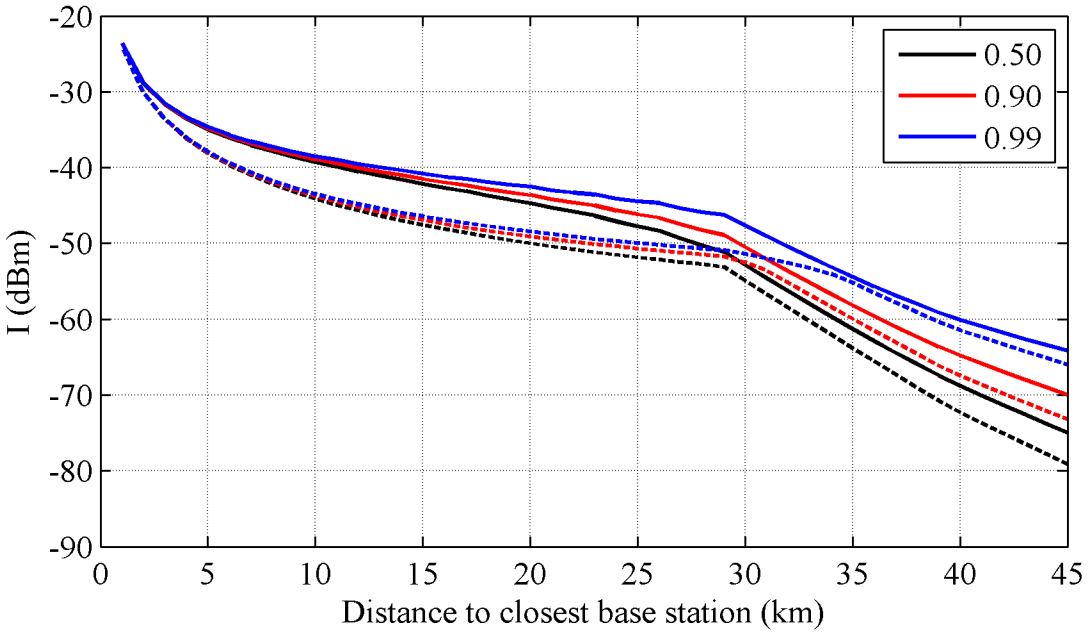

Figure 36. Probability I is less than ordinate. Aggregate (solid lines) versus single base station (dashed lines).

7 RADAR SNR

One of the key IPC is the baseline SNR. The baseline SNR determines radar performance without interference and influences the amount of interference power needed to degrade performance to the allowable level. Previous interference analyses have set SNR to a constant baseline level [3]. This approach, which we will refer to as constant SNR analysis, is applicable to short radar to target ranges where there is little or no path loss variability. However, at longer distances, atmospheric conditions introduce path loss variability and corresponding SNR variability. In this section we show how baseline SNR is determined and how a variable SNR can be included in interference analysis.

Situations that highlight where constant and variable SNR analyses are applicable are shown in Figure 37. Figures 37(a) and 37(b) illustrate situations where the radar to target path is short and constant SNR analysis is appropriate. Figure 37(c) illustrates a situation where the radar to target path is long and variable SNR analysis is appropriate. While constant SNR analysis is not accurate for long radar to target ranges, variable SNR analysis is accurate for all radar to target ranges. The main advantage of using a constant SNR is that it does not require radar to target link budget analysis.

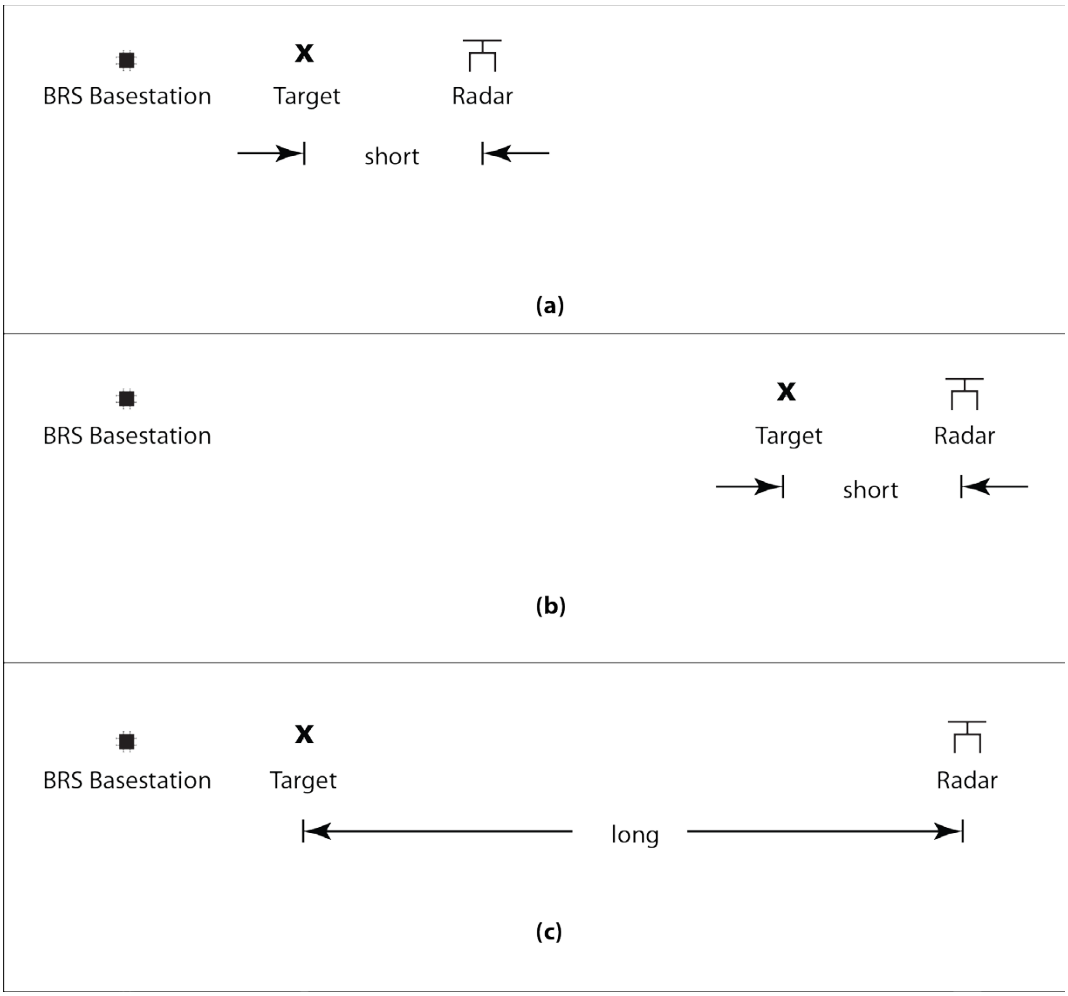

Figure 37. Short radar to target ranges as in (a) and (b) are analyzed with a constant SNR while long radar to target ranges as in (c) are analyzed with a variable SNR.

7.1 Definitions

Signal and noise powers are evaluated at the receiver input. The signal power is

$$s = \frac{1}{T}\int_{-T/2}^{T/2} s^2(t)dt \tag{12}$$

where T is the pulse period. The power is the average power while the pulse is on but may also be referred to as the peak power over the pulse repetition interval.

The receiver noise power is

$$n = \mathcal{E}\left\{\left(\int_{-\infty}^{\infty} n(\tau) h_{if}(t-\tau) d\tau\right)^2\right\} \tag{13}$$

where $\mathcal{E}\{\cdot\}$ is the expectation operator. When the noise power spectral density is constant,

$$n = kT_0 f_{rx} b_{if} \tag{14}$$

where k is Boltzman's constant, T_0 is the ambient temperature in degrees K, f_{rx} is the receiver noise factor, and b_{if} is the IF filter equivalent noise bandwidth.

The signal to noise ratio is

$$w = s/n \tag{15}$$

Finally capital letters S, N, and W correspond to s, n, and w in dB and script letters $\mathcal{S}$, $\mathcal{N}$, and $\mathcal{W}$ correspond to S, N, and W random variables.

7.2 Baseline SNR

Baseline SNR is the SNR needed to provide the $0.8\ P_d$ and $10^{-4}\ P_{fa}$ baseline performance level. It can be computed in a number of ways. The way we computed the ideal SNR and the SNR at the receiver input, which includes signal processing loss, is described in Appendix D.

With no integration, the ideal baseline SNR is 10.98 and 16.05 dB for non-fluctuating Swerling 0 and fluctuating Swerling 1 target RCSs, respectively. The corresponding SNR at the receiver input with 1.8 dB signal processing loss are 12.78 and 17.85, respectively.

Table 5 shows baseline SNR with integration for the various pulse widths and antenna rotation rates in the IEC 62388 standard. Short and medium baseline SNR are the same because their pulse repetition frequencies and bandwidths are identical.

Table 5. Baseline ideal SNR and SNR at receiver input for a 1.9 degree beam-width antenna at baseline performance $0.8\ P_d$ and $10^{-4}\ P_{fa}$. PW is pulse width, PRF is pulse repetition frequency, BW is IF filter bandwidth, RR is rotation rate, and n_p is the number of pulses integrated.

Pulse	PW (ns)	PRF (Hz)	BW (MHz)	RR (rpm)	n_p	Ideal SNR (dB)		SNR at receiver input (dB)	
						Swerling 0	Swerling 1	Swerling 0	Swerling 1
Short	50	1800	20	20	29	0.29	5.62	2.09	7.42
Short	50	1800	20	40	14	2.31	7.58	4.11	9.38
Medium	250	1800	20	20	29	0.29	5.62	2.09	7.42
Medium	250	1800	20	40	14	2.31	7.58	4.11	9.38
Long	800	785	3	20	12	2.75	8.01	4.55	9.81
Long	800	785	3	40	6	4.83	10.03	6.63	11.83

7.3 Variable SNR

This section describes a variable SNR analysis method. The method is demonstrated with the set of targets described in the IEC 62388 standard clutter free test [16], [21] and SNR distributions determined by the ITM propagation model.

We start by creating a link budget expression for the radar's received power and use it to compute the received power for the targets in the IEC 62388 standard clutter free test. It will be shown that the SNR for all targets in the clutter free test is in excess of that needed for baseline performance. We assume that the excess power margin is needed to compensate for reduced RCS due to different target aspects, shapes, and construction materials and remove it prior to interference tests by decreasing the RCS.

7.3.1 Link Budget

For free space, i.e. propagation in an empty vacuum, the radar's received power is

$$s = \frac{p_{tx} g}{4\pi d_{rt}^2} \cdot \frac{\sigma_{av}}{4\pi d_{rt}^2} \cdot a_e \tag{16}$$

where p_{tx} is the peak transmitted power, g is the radar antenna gain relative to an isotropic antenna, σ_{av} is the target average or mean RCS in square meters, d_{rt} is the distance from the radar to the target in meters, and a_e is the effective antenna aperture in square meters. The $4\pi d^2$ terms in the denominator indicate that the transmitted signal and the signal reflected off the target spread isotropically.

But it can be shown that the aperture of an antenna is related to the gain of an antenna relative to an isotropic radiator by

$$a_e = \frac{g\lambda^2}{4\pi} \tag{17}$$

where λ is the wavelength, so

$$s = \frac{p_{tx} g}{4\pi d_{rt}^2} \cdot \frac{\sigma_{av}}{4\pi d_{rt}^2} \cdot \frac{g\lambda^2}{4\pi} \tag{18}$$

and

$$s = \frac{p_{tx} g^2 \sigma_{av} \lambda^2}{(4\pi)^3 d_{rt}^4} \tag{19}$$

To emulate practical terrestrial propagation conditions we introduce the excess path loss factor, a which is dependent on d_{rt}. The factor is assumed to be completely correlated between the outbound path from the radar to the target and the inbound path from the target to the radar. Consequently it is squared in the link budget equation

$$s = \frac{p_{tx} g^2 \sigma_{av} \lambda^2}{(4\pi)^3 d_{rt}^4 a^2} \tag{20}$$

Finally adding in the radar losses to refer power to the receiver input

$$s = \frac{p_{tx} g^2 \sigma_{av} \lambda^2}{(4\pi)^3 d_{rt}^4 a^2 l_d l_{bm} l_{ct} l_{cr}} \tag{21}$$

Since s is evaluated at the receiver input, receiver signal losses, l_{sp}, are not included.

7.3.2 SNR for the IEC 62388 Standard Test Cases

Table 6 shows the SNR for the free space channel where the excess path loss, a, is 1. To limit the scope of the problem we only use pulse widths that satisfy range limits shown in Figure 9 and provide the highest SNR.

Figure 38 shows the SNR distributions, $Pr\{\mathcal{W} > W\}$ using ITM where a is random. Cases 1–9 use the long pulse and case 10 uses the short pulse. Table 7 summarizes various quantiles. Case 10 has the shortest range and an approximately constant SNR while case 1 has the longest range and the most variability. Clearly variability increases with radar to target range.

Table 6. IEC 62388 standard clutter free test case SNR in free space channel. Shaded cells indicate pulse meets target range requirement.

Case	Target	Height (m)	Range		RCS (m^2)	FS SNR (dB)		
			nmi	km		Pulse width		
						Short	Med	Long
1	60m high shoreline	50.0	20.0	37.0	50000.0	27.9	27.9	36.1
2	6 m high shoreline	5.0	8.0	14.8	5000.0	33.8	33.8	42.0
3	3 m high shoreline	2.5	6.0	11.1	2500.0	35.8	35.8	44.0
4	SOLAS ship > 5000gt	10.0	11.0	20.4	30000.0	36.1	36.1	44.3
5	SOLAS ship > 500gt	5.0	8.0	14.8	1000.0	26.8	26.8	35.1
6	Small boat with reflector	4.0	3.7	6.8	0.5	7.2	7.2	15.4
7	Buoy with reflector	3.5	3.6	6.7	1.0	10.7	10.7	18.9
8	Buoy	3.5	3.0	5.6	0.5	10.8	10.8	19.1
9	Small 10 m boat	2.0	3.0	5.6	1.4	15.3	15.3	23.6
10	Channel marker	1.0	1.0	1.9	0.1	22.9	22.9	31.2

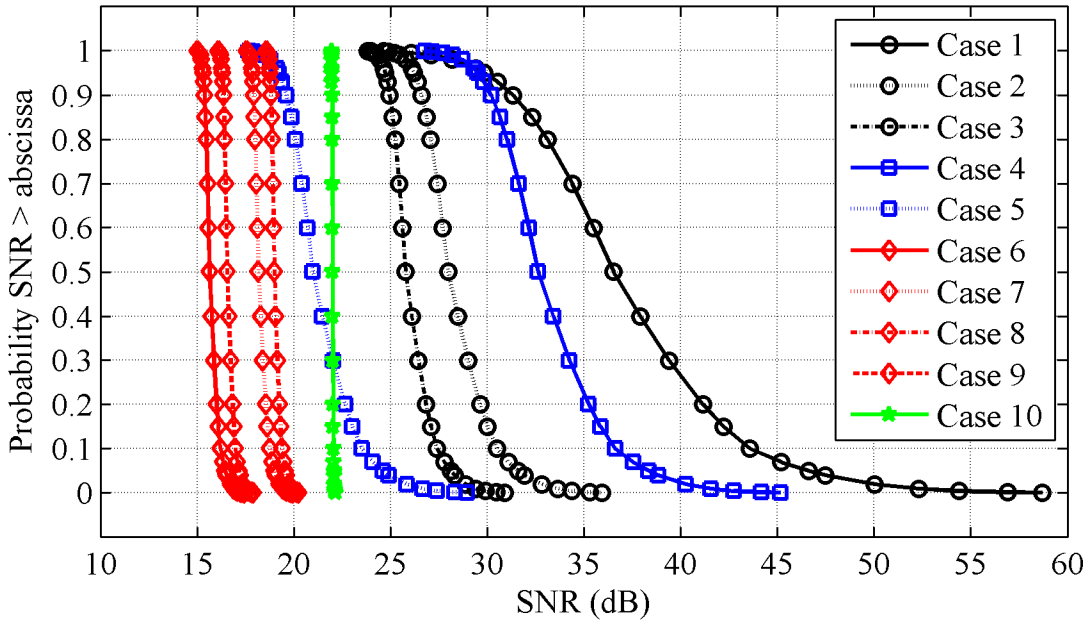

Figure 38. SNR distributions using the ITM for 10 IEC 62388 standard clutter free test cases.

Table 7. IEC 62388 standard clutter free test case SNR quantiles using the ITM.

Case	Description	Height (m)	Range		RCS m^2	Pulse	FS SNR (dB)	ITM SNR (dB) $Pr\{W > W\}$				
			nmi	km				0.50	0.80	0.90	0.95	0.99
1	60m high shoreline	50.0	20.0	37.0	50000.0	Long	36.1	36.5	33.1	31.3	29.8	27.1
2	6 m high shoreline	5.0	8.0	14.8	5000.0	Long	42.0	28.0	27.1	26.6	26.2	25.5
3	3 m high shoreline	2.5	6.0	11.1	2500.0	Long	44.0	25.8	25.2	25.0	24.7	24.3
4	SOLAS ship > 5000gt	10.0	11.0	20.4	30000.0	Long	44.3	32.6	31.0	30.2	29.5	28.2
5	SOLAS ship > 500gt	5.0	8.0	14.8	1000.0	Long	35.1	21.0	20.1	19.6	19.2	18.5
6	Small boat with reflector	4.0	3.7	6.8	0.5	Long	15.4	15.6	15.5	15.4	15.3	15.2
7	Buoy with reflector	3.5	3.6	6.7	1.0	Long	18.9	18.2	18.0	17.9	17.8	17.7
8	Buoy	3.5	3.0	5.6	0.5	Long	19.1	19.0	18.9	18.8	18.8	18.7
9	Small 10 m boat	2.0	3.0	5.6	1.4	Long	23.6	16.5	16.4	16.4	16.3	16.2
10	Channel marker	1.0	1.0	1.9	0.1	Short	22.9	22.0	22.0	22.0	22.0	22.0

7.3.3 Excess Power Margin

We define the excess power margin as the ratio of the SNR exceeded 99% of the time to the baseline SNR

$$m = {}^{w_{99}}/_{w_b} \tag{22}$$

where w_{99} is the SNR exceeded 99% of the time and w_b is the baseline SNR. Note that the SNR exceeded 99% of the time is limited by fading and not ducting enhancement.

Assuming the mean RCS varies with target aspect, shape, and construction materials we remove the excess power margin by reducing the mean RCS by

$$\hat{\sigma}_{av} = {}^{\sigma_{av}}/_{m} \tag{23}$$

The radar link budget with the excess power margin removed is now

$$s = \frac{p_{tx} g^2 \sigma_{av} \lambda^2}{(4\pi)^3 d_{rt}^4 a^2 l_d l_{bm} l_{ct} l_{cr} m} \tag{24}$$

Table 8 shows the free space and ITM 99% SNR power margins for the IEC 62388 standard clutter free test cases. The table shows maximum FS margin of 32.5 dB for case 4 i.e. the SOLAS ship > 5000 gt. This corresponds to the standard which states the RCS may be reduced as much as 30 dB because of target aspect, shape, or constructions materials and justifies removal of the excess SNR by reducing the RCS prior to interference analysis. The corresponding ITM 99% margin is only 16.4 dB. The smaller margin is caused by the ITM 99% SNR being less than the FS SNR.

Figure 39 shows the SNR distributions with the excess power margin removed so that the baseline SNR is exceeded 99% of the time. Finally, Table 9 shows the reduced RCSs. The RCS for case 4 was reduced 16.4 dB to 691.3 square meters from 30000. This reduction is commensurate with the measured RCS discussed in Section 4.3 .

Table 8. IEC 62388 standard clutter free test case power margins.

Case	Description	Height (m)	Range		Baseline SNR (dB)	FS SNR (dB)	FS Margin (dB)	ITM 99% SNR (dB)	ITM 99% Margin (dB)
			nmi	km					
1	60 m high shoreline	50.0	20.0	37.0	11.83	36.1	24.27	27.1	15.2
2	6 m high shoreline	5.0	8.0	14.8	11.83	42.0	30.17	25.5	13.6
3	3 m high shoreline	2.5	6.0	11.1	11.83	44.0	32.17	24.3	12.5
4	SOLAS ship > 5000gt	10.0	11.0	20.4	11.83	44.3	32.5	28.2	16.4
5	SOLAS ship > 500gt	5.0	8.0	14.8	11.83	35.1	23.3	18.5	6.7
6	Small boat with reflector	4.0	3.7	6.8	11.83	15.4	3.6	15.2	3.3
7	Buoy with reflector	3.5	3.6	6.7	11.83	18.9	7.1	17.7	5.9

Case	Description	Height (m)	Range		Baseline SNR	FS SNR	FS Margin	ITM 99% SNR	ITM 99% Margin
8	Buoy	3.5	3.0	5.6	11.83	19.1	7.3	18.7	6.8
9	Small 10 m boat	2.0	3.0	5.6	11.83	23.6	11.8	16.2	4.4
10	Channel marker	1.0	1.0	1.9	9.38	22.9	13.5	22.0	12.6

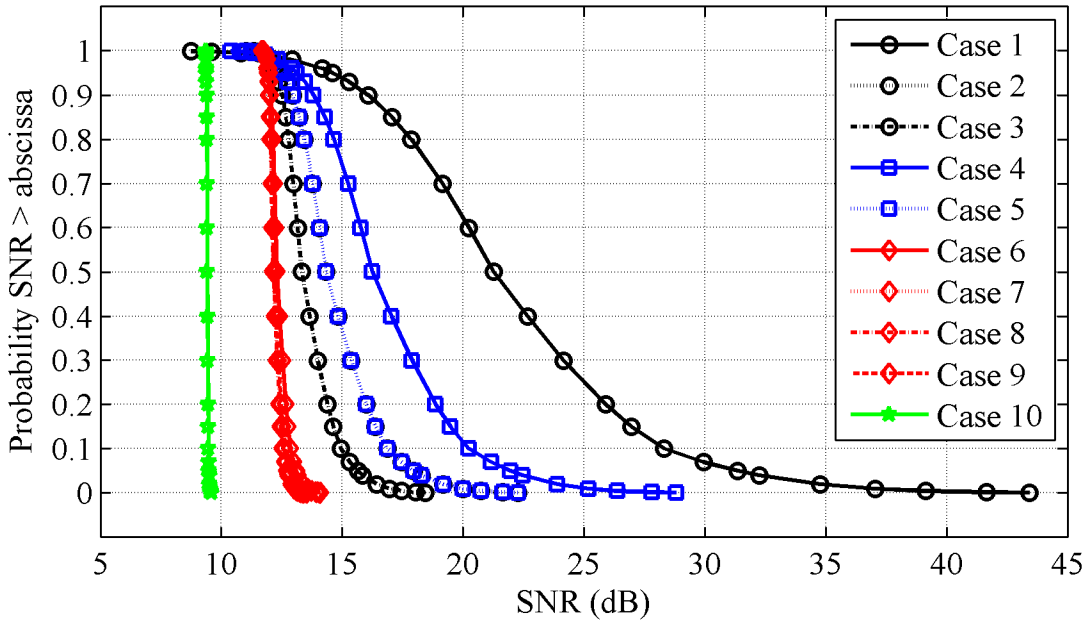

Figure 39. SNR distributions for 10 IEC 62388 standard clutter free test cases with excess power margin removed. There are 3 fewer curves visible because cases 2 and 5, 6 and 7, and 8 and 9 have similar target parameters.

Table 9. Reduced mean RCS for IEC 62388 standard test cases.

Case	Description	99%Margin (dB)	σ_{av}		$\hat{\sigma}_{av}$	
			m^2	dBsm	m^2	dBsm
1	60 m high shoreline	15.2	50000	46.98	1492.7	31.7
2	6 m high shoreline	13.6	5000	36.98	216.2	23.3
3	3 m high shoreline	12.5	2500	33.97	142.0	21.5
4	SOLAS ship > 5000gt	16.4	30000	44.77	691.3	28.4
5	SOLAS ship > 500gt	6.7	1000	30.00	216.2	23.3
6	Small boat with reflector	3.3	0.5	-3.01	0.232	-6.4
7	Buoy with reflector	5.9	1.0	0.00	0.258	-5.9
8	Buoy	6.8	0.5	-3.01	0.103	-9.9
9	Small 10 m boat	4.4	1.4	1.46	0.512	-2.9
10	Channel marker	12.6	0.1	-10.0	0.006	-22.6

8 CONCLUSION

This report provides background information needed to analyze effects of BRS reallocation on 2900–3100 MHz band marine radars. Key topics covered are interference protection criteria (IPC), interference scenario, and the various system and propagation models.

Comprehensive IPC include performance levels, powers, and reliabilities for baseline (interference-free) and allowable degraded conditions. Reliability in this context is determined solely by radio wave propagation path loss variability caused by terrain and atmospheric conditions and is independent of electrical or mechanical malfunction.

The interference scenario consists of a maritime radar target such as a boat or buoy between a network of base stations and a ship with a maritime radar. Magnetron radar and radar target models are derived from the IEC 62388 standard for shipborne radars. BRS system models are derived from WiMAX and LTE standards. Radio wave propagation is modelled with the ITS Irregular Terrain Model (ITM) because of its ability to model path loss variability.

A BRS base station signal was measured and statistically characterized. The signal statistics were found to be nearly Gaussian in the necessary bandwidth and Gaussian in the spurious domain. Statistics in the necessary bandwidth are considered nearly Gaussian because of a slight drop in peak signal levels. The roll-off or OOB regions between the necessary bandwidth and spurious regions were not measured due to measurement system dynamic range considerations. Pending future measurements, we are assuming OOB emissions are Gaussian as well. Consequently, it is reasonable to model the BRS signal as Gaussian noise. This finding greatly simplifies analysis of interference in marine radars from base station unwanted emissions.

Statistical characterization was done on measurements in a wide bandwidth. However, since the statistics are Gaussian they should also be Gaussian when the BRS signal is filtered to a narrower bandwidth and when any number of BRS signals are added to represent the signal from an aggregate of base stations.

A method for computing aggregate interference power distributions using the radio wave propagation model and Monte Carlo analysis was developed. These distributions are essential for analyzing radar link reliability. Because of the radar antenna's narrow azimuthal beam width, maximum aggregate interference power was found to come from base stations along a line formed by the most closely repetitively-spaced base stations. The aggregate interference power was found to be as much as 6 dB greater than the power from a single base station. Hence it is important that interference analysis be done with an aggregate of base stations.

Although interference path loss variability is usually included in interference analysis, desired path loss variability often is not. In the maritime radar case the desired path is the radar to target path. In devising a method for including radar to target path loss variability into our analysis we found excess SNR in the radar to target link budgets used for industry acceptance tests. Although this excess SNR could potentially mitigate interference, we found that it is needed to accommodate reductions in target mean RCS due to changes in target aspect, shape, and construction materials. Consequently we recommend removing the excess SNR by reducing mean RCS prior to interference analysis.

9 ACKNOWLEDGEMENTS

This work was sponsored by the U.S. Coast Guard Spectrum Management Telecommunications Policy Division, U.S. Coast Guard CG-652, 2100 2nd St. SW Stop 7101, Washington DC 20593-7101. The authors would like to acknowledge Fred Mistichelli (former Division Chief), Joseph Hersey (former Division Chief), and Daniel Freedman (former Spectrum Engineer) for their sponsorship.

The authors would also like to acknowledge David Turnage, Research and Development Manager, Kelvin Hughes Ltd.; Lawrence Cohen, Electronics Engineer, U.S. Naval Research Laboratory; Jon Higham, Program Coordinator, United Kingdom Office of Communication (OFCOM); David G. Money, consultant to the OFCOM; Richard Rees, Spectrum Policy and Technical Standards Manager, United Kingdom Maritime and Coastal Agency; and David Blevins, Senior Staff Engineer, Northrup Grumman Marine Systems, for sharing their insights into this issue.

Finally, the authors would like to acknowledge Geoffrey Sanders, of the Institute for Telecommunication Sciences, for his contributions towards measuring WiMAX signal characteristics and Al Romero, Visual Information Specialist, of the National Oceanic and Atmospheric Administration (NOAA), for creating the illustrative figures.

10 REFERENCES

[1] International Telecommunication Union, "Procedures for determining the potential for interference between radars operating in the radiodetermination service and systems in other services," Recommendation ITU-R M.1461-1, July 2003.

[2] International Telecommunication Union, "Tests illustrating the compatibility between maritime radionavigation radars and emissions from radiolocation radars in the band 2900–3100 MHz," Report ITU-R M.2032, 2003.

[3] F. Sanders et. al., "Effects of RF interference on radar receivers," NTIA Report TR-06-444, September 2006, http://www.its.bldrdoc.gov/publications/2481.aspx.

[4] J.E. Carroll, G.A. Sanders, F.H. Sanders, and R.L. Sole, "Case study: Investigation of interference into 5 GHz weather radars from unlicensed national information infrastructure devices, Part I," NTIA Technical Report TR-11-473, November 2010, http://www.its.bldrdoc.gov/publications/2548.aspx.

[5] A. Paul et. al., "Interference protection criteria," NTIA Report 05-432, October 2005, http://www.its.bldrdoc.gov/publications/2462.aspx.

[6] International Telecommunication Union, "Studies on frequency-related matters on International Mobile Telecommunications and other terrestrial mobile broadband applications," Resolution 233 (WRC-12),The World Radiocommunication Conference (Geneva, 2012).

[7] International Electrotechnical Commission, "Maritime navigation and radiocommunication equipment and systems – Shipborne radar – Performance requirements, methods of testing and required test results," IEC 62388, Edition 1.0, 2007-12.

[8] International Maritime Organization, "Adoption of the revised performance standards for radar equipment," Annex 34, Resolution MSC.192(79), December 6, 2004.

[9] Institute of Electrical and Electronic Engineers, "IEEE recommended practice for the analysis of in-band and adjacent band interference and coexistence between radio systems," IEEE Std 1900.2-2008, July 29, 2008.

[10] United Kingdom of Great Britain and Northern Ireland, "Radar adjacent band selectivity," Recommendation ITU-R 5b/389-E, November 18, 2009.

[11] U.S. Department of Commerce, National Telecommunications and Information Administration, "An assessment of the near-term viability of accommodating wireless broadband systems in the 1675–1710 MHz, 1755–1780 MHz, 3500–3650 MHz, and 4200–4220 MHz, 4380–4400 MHz bands," October 2010, http://www.ntia.doc.gov/files/ntia/publications/fasttrackevaluation_11152010.pdf.

[12] European Telecommunications Standards Institute, "Technical Specification, Digital cellular telecommunications system (Phase 2+); Universal Mobile Telecommunications

System (UMTS); LTE; E-UTRA,UTRA, and GSM/Edge; Multi-Standard Radio (MSR) Base Station (BS) radio transmission and reception," ETSI TS 137 104 version 11.2.1 Release 11, Oct. 2012.

[13] International Telecommunication Union Joint Task Group 4-5-6-7, Appendix 1 "Characteristics of terrestrial IMT-Advanced systems for frequency sharing/interference analyses" in Attachment 1, "Protection criteria, system characteristics, related materials on modelling considerations and sharing studies already performed or underway in ITU-R related to the terrestrial services" in Annex 2 "Compilation of material maintained by the Joint Task Group 4-5-6-7 working groups" of Report on the Fourth meeting of the Joint Task Group 4-5-6-7, Document 4-5-6-7/393-E, October 30, 2013.

[14] WiMAX Forum, "Mobile WiMAX – Part 1: A Technical Overview and Performance Evaluation," WiMAX Forum white paper, August 2006.

[15] International Electrotechnical Commission, Assessment of target detection in clutter in "Maritime navigation and radiocommunication equipment and systems – Shipborne radar – Performance requirements, methods of testing and required test results," IEC 62388, Edition 1.0, 2007-12, Section 5.9.3, p. 40.

[16] International Electrotechnical Commission, Table 2 - Range of first detection in minimal clutter in "Maritime navigation and radiocommunication equipment and systems – Shipborne radar – Performance requirements, methods of testing and required test results," IEC 62388, Edition 1.0, 2007-12, Section 5.9.2, p. 38.

[17] International Electrotechnical Commission, Table D.6 – Additional radar system parameters in "Maritime navigation and radiocommunication equipment and systems – Shipborne radar – Performance requirements, methods of testing and required test results," IEC 62388, Edition 1.0, 2007-12, Appendix D, pp. 154.

[18] International Electrotechnical Commission, Table D.8 - S-band radar parameters in "Maritime navigation and radiocommunication equipment and systems – Shipborne radar – Performance requirements, methods of testing and required test results," IEC 62388, Edition 1.0, 2007-12, Appendix D, pp. 156.

[19] A. Toskala and T. Lunttila, "OFDMA Basics," Chapter 4.3 of *LTE for UMTS – Evolution to LTE-Advanced*, H. Holma and A. Toskala, Eds., Second Edition, New York: Wiley, 2011, pp. 70-76.

[20] D. Astely, E. Dahlman, A. Furuskar, Y. Jading, M. Lindstrom, and S. Parkvall, "LTE: The evolution of mobile broadband," *IEEE Communication Magazine*, April 2009, pp. 44–51.

[21] International Electrotechnical Commission, Table D.7 – Target size, height, and RCS values in "Maritime navigation and radiocommunication equipment and systems – Shipborne radar – Performance requirements, methods of testing and required test results," IEC 62388, Edition 1.0, Section 5.9.2, 2007-12, p 155.

[22] P.L. Rice, A.G. Longley, K.A. Norton, and A.P. Barsis, "Transmission loss predictions for tropospheric communication circuits," National Bureau of Standards Technical Note 101,Vol. 1, pp.10-14 to 10-18, Revised January 1, 1967, http://www.its.bldrdoc.gov/publications/2726.aspx.

[23] P. Swerling, "Probability of detection for fluctuating targets," *IRE Transactions on Information Theory*, vol. 6, no. 2, April 1960, pp. 269–308.

[24] E.F. Knott, J. Shaeffer, Michael Tuley, *Radar Cross Section*, Second Edition, SciTech Publishing, 2004, Raleigh, N.C., pp. 258-260.

[25] P.D.L. Williams, H.D. Cramp, and K. Curtis, "Experimental study of the radar cross section of maritime targets," *Electronic Circuits and Systems*, July 1978, pp. 121–135.

[26] M. Cotton, R. Achatz, J. Wepman, and B. Bedford, "Interference potential of ultrawideband signals, Part 1: Procedures to characterize ultrawideband emissions and measure interference susceptibility of C-band satellite digital television receivers," NTIA Report TR-05-419, February 2005, http://www.its.bldrdoc.gov/publications/2449.aspx.

[27] M. Cotton, R. Achatz, J. Wepman, and P. Runkle, "Interference potential of ultrawideband signals, Part 2: Measurements of gated Gaussian noise interference to C-band satellite digital television receivers," NTIA Report TR-05-429, August 2005, http://www.its.bldrdoc.gov/publications/2459.aspx.

[28] Frank H. Sanders, Robert L. Sole, John E. Carroll, Glenn S. Secrest, T. Lynn Allmon, "Analysis and Resolution of RF Interference to Radars Operating in the Band 2700-2900 MHz from Broadband Communication Transmitters," NTIA Technical Report TR-13-490, October 2012, http://www.its.bldrdoc.gov/publications/2684.aspx.

[29] ITU-R, "Unwanted emissions in the spurious domain," Recommendation ITU-R SM.329-10, February 2003.

[30] M. Cotton, R. Achatz, J. Wepman, and B. Bedford, "Dynamic range of the vector network analyzer", Appendix E in "Interference Potential of Ultrawideband Signals, Part 1: Procedures to characterize ultrawideband emissions and measure interference susceptibility of C-band satellite digital television receivers," NTIA Report TR-5-419, February 2005, http://www.its.bldrdoc.gov/publications/2449.aspx.

APPENDIX A: ANALYSIS PARAMETERS

Analysis parameters are provided in the following tables. Radar and target parameters are taken from the IEC standard [A-1], [A-2], [A-3], [A-4]. BRS base station parameters are derived from the ITU [A-5] and WiMAX forum [A-6]. The radio wave propagation ITM parameters are defined in [A-7].

Table A-1. Physical parameters.

Parameter	**Value**	**Note**
Climate	Maritime temperate	
Terrain	Sea/Coastal	
Precipitation	No	IEC 62388 standard clutter free test
Radar sea clutter	No	IEC 62388 standard clutter free test
Radar precipitation clutter	No	IEC 62388 standard clutter free test
Radar target fluctuation	Swerling 1	IEC 62388 standard clutter free test

Table A-2. IEC 62388 standard clutter free test target physical parameters

Case	**Target**	**Height (m)**	**Range**		**RCS (m^2)**
			(nmi)	(km)	
1	60 m high shoreline	50.0	20.0	37.0	50000.0
2	6 m high shoreline	5.0	8.0	14.8	5000.0
3	3 m high shoreline	2.5	6.0	11.1	2500.0
4	SOLAS ship > 5000gt	10.0	11.0	20.4	30000.0
5	SOLAS ship > 500gt	5.0	8.0	14.8	1000.0
6	Small boat with reflector	4.0	3.7	6.8	0.5
7	Buoy with reflector	3.5	3.6	6.7	1.0
8	Buoy	3.5	3.0	5.6	0.5
9	Small 10 m boat	2.0	3.0	5.6	1.4
10	Channel marker	1.0	1.0	1.9	0.1

Table A-3. IEC 62388 standard clutter free test radar parameters not related to pulse width.

Parameter	**Value**	**Note**
Center frequency	3050 MHz	
Source power	30 kW	
Integration	Non-coherent	
Antenna azimuth beam width	1.9 degrees	
Antenna rotation rate	40 revolutions/minute	
Antenna polarization	Horizontal	
Antenna gain	27.0 dB	
Antenna height	15 m	
Receiver noise figure	5.0 dB	Referred to limiter input

Parameter	Value	Note
Antenna radome loss	1.0 dB	Transmit and receive
Receiver circuit loss	2.7 dB	
Transmitter circuit loss	2.7 dB	
Signal processing loss	1.8 dB	
Integration beam shape loss	1.6 dB	Transmit and receive

Table A-4. IEC 62388 standard clutter free test pulse width and related parameters

Descriptor	Width (ns)	Pulse repetition frequency (Hz)	Receiver bandwidth (MHz)
Short	50	1800	20
Medium	250	1800	20
Long	800	785	3

Table A-5. BRS macro base station parameters for 10 MHz bandwidth signal.

Parameter	Units	Report	WiMax Forum	ITU WP-5D			Note
				Rural	Suburban	Urban	
Cell radius	km	1.5	1.4	> 2	0.4-2.5	0.2-0.8	
Antenna height	m	30	32	30	25	20	
Sectorization	sectors	3	3	3	3	3	
Down-tilt	degrees	3.5	3	3	6	10	
Frequency reuse		1	NA	1	1	1	
Horizontal beam width	degrees	65	70	65	65	65	
Vertical beam width	degrees	12.0	14.0	7.5	12.0	12.0	1
Antenna polarization		Slant linear	NA	Slant linear	Slant linear	Slant linear	2
Feeder loss	dB	3	3	3	3	3	3
Maximum base station output power	W	40	40	40	40	40	3,4
Maximum antenna gain	dBi	16	15	18	16	16	

Note 1: Calculated from equations in Recommendation ITU-R F.1336 [A-8].

Note 2: ±45 degree slant also referred to as cross linear polarization

Note 3: WiMAX Forum specifications did not include feeder loss. Maximum base station output power was increased by an assumed 3 dB feeder loss to compensate.

Note 4: Maximum power amplifier output.

Table A-6. BRS macro base station effective radiated power.

Parameter	Units	Report	WiMax Forum	ITU WP-5D			Note
				Rural	Suburban	Urban	
Maximum base station output power	dBmW	46	46	46	46	46	
Feeder loss	dB	3	3	3	3	3	
Maximum antenna gain	dBi	16	15	18	16	16	
Downtilt loss	dB	1	0.5	2	3	8	1
Effective antenna gain	dBi	15	14.5	16	13	8	2
Effective radiated power	dBmW	58	57.5	59	56	51	

Note 1: Calculated from mechanical tilt and peak gain equations in Recommendation ITU-R F.1336 [A-8].

Note 2: Effective antenna gain is maximum antenna gain minus downtilt loss.

Table A-7. ITM parameters. Base station is the transmitter and radar is the receiver.

Parameter	Value	Note
Frequency (MHz)	3050	
Radio climate surface refractivity (Ns)	325	1
Ground conductivity (S/M)	0.005 (land), 5.0 (sea)	
Ground dielectric constant	15.0 (land), 81.0 (sea)	
Delta h (meters)	0	Terrain irregularity, 2
Effective earth radius factor	1.4	
Polarization	Vertical	
Transmitter site criteria	Random	3
Receiver site criteria	Random	3
Radio climate	North America marine temperate	

Note 1: Average of continental temperate (301) and marine temperate (350).

Note 2: Forces location variability to 0 leaving only time variability.

Note 3: Random used so effective height is the same as actual height above sea level.

A.1 References

[A-1] International Electrotechnical Commission, Table D.6 – Additional radar system parameters in “Maritime navigation and radiocommunication equipment and systems – Shipborne radar – Performance requirements, methods of testing and required test results,” IEC 62388, Edition 1.0, 2007-12, Appendix D, pp. 154.

[A-2] International Electrotechnical Commission, Table D.8 - S-band radar parameters in “Maritime navigation and radiocommunication equipment and systems – Shipborne radar

– Performance requirements, methods of testing and required test results," IEC 62388, Edition 1.0, 2007-12, Appendix D, pp. 156.

[A-3] International Electrotechnical Commission, Table 2 - Range of first detection in minimal clutter in "Maritime navigation and radiocommunication equipment and systems – Shipborne radar – Performance requirements, methods of testing and required test results," IEC 62388, Edition 1.0, 2007-12, Section 5.9.2, p. 38.

[A-4] International Electrotechnical Commission, Table D.7 – Target size, height, and RCS values in "Maritime navigation and radiocommunication equipment and systems – Shipborne radar – Performance requirements, methods of testing and required test results," IEC 62388, Edition 1.0, Section 5.9.2, 2007-12, p 155.

[A-5] International Telecommunication Union Joint Task Group 4-5-6-7, Appendix 1 "Characteristics of terrestrial IMT-Advanced systems for frequency sharing/interference analyses" in Attachment 1, "Protection criteria, system characteristics, related materials on modelling considerations and sharing studies already performed or underway in ITU-R related to the terrestrial services" in Annex 2 "Compilation of material maintained by the Joint Task Group 4-5-6-7 working groups" of Report on the Fourth meeting of the Joint Task Group 4-5-6-7, Document 4-5-6-7/393-E, October 30, 2013.

[A-6] WiMAX Forum, Table 7: Mobile WiMAX System Parameters and Table 10: DL Link Budget for Mobile WiMAX in "Mobile WiMAX – Part 1: A Technical Overview and Performance Evaluation," WiMAX Forum white paper, August 2006, pp. 31-33.

[A-7] G.A. Hufford, A.G. Longley, and W.A. Kissick, "A Guide to the Use of the ITS Irregular Terrain Model in the Area Prediction Mode," NTIA Report 82-100, April 1982, http://www.its.bldrdoc.gov/publications/2091.aspx.

[A-8] International Telecommunication Union, Reference radiation patterns of omnidirectional, sectoral and other antennas in point-to-multipoint systems for use in sharing studies in the frequency range from 1 GHz to about 70 GHz, Recommendation ITU-R F.1336-3, March 2012.

APPENDIX B: PROPAGATION MODELS

B.1 Free Space Model

The free space (FS) model assumes the radio wave is transmitted into an empty vacuum. Practically, we use it when the radio wave is not expected to interact with the atmosphere or objects such as the earth.

With the FS model the propagation path loss is

$$l_{fs} = \left(\frac{4\pi d}{\lambda}\right)^2 \tag{B-1}$$

and the corresponding distance is

$$d = \frac{\lambda\sqrt{l_{fs}}}{4\pi} \tag{B-2}$$

where λ is the wavelength in the same units as d.

B.2 General Propagation Models

There are a number of general propagation models used for practical terrestrial propagation paths with irregular terrain and atmospheric effects. These models characterize path loss as

$$l_p = l_{fs}a \tag{B-3}$$

where a is the excess path loss due to line of sight, diffraction, and scattering losses, or in dB

$$L_p(dB) = L_{fs} + A\,. \tag{B-4}$$

The excess path loss covers both signal fading and signal enhancement and is modeled as a random variable whose statistics vary with location and time. The location variability is due to terrain and the time variability is due to atmospheric effects. In the maritime case, location variability is insignificant but time variability is important.

Table B-1 lists some commonly used general propagation models including Recommendation ITU-R P.1812 [B-1], ITU-R P.1546 [B-2], and ITU-R P.452 [B-3] models, used by the ITU-R, and the ITS Irregular Terrain Model (ITM) [B-4], [B-5], [B-6], [B-7] used by the ITS. The models are valid over the listed frequency range. All account for smooth earth diffraction and so are valid at distances beyond the radio horizon. Unless otherwise noted, the models include tropospheric scatter, surface ducting, and elevated ducting.

Among the many differences in these models, the features that were most important to us were the mode of operation, i.e. point-to-point or point-to-area, and excess attenuation. Our analysis

requires point to area mode with both fading and enhancement. ITS-ITM was the only propagation model that satisfied these requirements.

Table B-1. General propagation models. P2P is point-to-point mode and P2A is point-to-area mode.

Model	Frequency range	P2P	P2A	Fading	Enhancement	Note
ITU-R P.1812	30 MHz-3 GHz	Yes	No	No	Yes	No gaseous absorption
ITU-R P.452	700 MHz-50 GHz	Yes	No	No	Yes	
ITS-ITM	20 MHz-20 GHz	Yes	Yes	Yes	Yes	
ITU-R P.1546	30 MHz-3 GHz	No	Yes	No	Yes	

B.3 References

[B-1] International Telecommunication Union, “A path-specific propagation prediction method for point-to-area terrestrial services in the VHF and UHF bands,” Recommendation ITU-R P.1812-2, February 2012.

[B-2] International Telecommunication Union, “Method for point-to-area predictions for terrestrial services in the frequency range 30 MHz to 3000 MHz,” Recommendation ITU-R P.1546-4, October 2009.

[B-3] International Telecommunication Union, “Prediction procedure for the evaluation of interference between stations on the surface of the Earth at frequencies above about 0.1 GHz,” Recommendation ITU-R P.452-14, October 2009.

[B-4] P.L. Rice, A.G. Longley, K.A. Norton, and A.P. Barsis,”Transmission loss predictions for tropospheric communication circuits,” NBS Technical Note 101, Vol. I, Jan. 1, 1967, http://www.its.bldrdoc.gov/publications/2726.aspx.

[B-5] P.L. Rice, A.G. Longley, K.A. Norton, and A.P. Barsis,”Transmission loss predictions for tropospheric communication circuits,” NBS Technical Note 101, Vol. II, Jan. 1, 1967, http://www.its.bldrdoc.gov/publications/2727.aspx.

[B-6] A.G. Longley and P.L. Rice, “Prediction of tropospheric radio transmission loss over irregular terrain,” ESSA Tech. Report ERL 79-ITS 67, July 1968, http://www.its.bldrdoc.gov/publications/2784.aspx.

[B-7] G.A. Hufford, A.G. Longley, and W.A. Kissick, “A Guide to the use of the ITS irregular terrain model in the area prediction mode,” NTIA Report 82-100, April 1982, http://www.its.bldrdoc.gov/publications/2091.aspx.

APPENDIX C: IRREGULAR TERRAIN MODEL

The Irregular Terrain Model (ITM) radio wave propagation model [C-1]–[C-4] characterizes path loss, l_p, as a random variable. The randomness is due to changes in time, location, and situation.[3] Mathematically the path loss is

$$l_p = l_{fs} a \tag{C-1}$$

where l_{fs} is free space loss and a is the excess path-loss or attenuation random variable. Written in decibels we have

$$L_p(dB) = L_{fs} + A\,. \tag{C-2}$$

The random variable A is defined as

$$A = \begin{cases} A' & if\ A' > 0 \\ A'\left(\dfrac{29 - A'}{29 - 10A'}\right) & otherwise \end{cases} \tag{C-3}$$

where

$$A' = A_{ref} - V_{med} - Y_T - Y_L - Y_S. \tag{C-4}$$

A_{ref} is the reference attenuation that characterizes line of sight, diffraction, and scatter loss, V_{med} is a climatic adjustment to the reference attenuation, and Y_T, Y_L, and Y_S are time, location, and situation variability deviates. All factors are dependent on distance and climate.

The attenuation for a specific fraction of times, locations, and situations is written as $A(q_T, q_L, q_S)$. In the maritime temperate climate, variability in either location or situation is minimal so we are left with only time variability which we abbreviate $A(q_T)$ and is computed from

$$A' = \mu - Y_T \tag{C-5}$$

where $\mu = A_{ref} - V_{med}$.

The time variability deviate, Y_T, is zero mean and log normally distributed

$$f(Y_T) = \frac{1}{\sqrt{2\pi}\sigma} exp\left(\frac{-Y_T^2}{2\sigma^2}\right). \tag{C-6}$$

[3] Situation refers to considerations not accounted for by other model parameters such as receiver design, antenna mounting, and operator experience.

In terms of the standard normal deviate, z_T, we have

$$Y_T(q_T) = \sigma_T z_T \tag{C-7}$$

where

$$q_T = Pr\{Z_T \geq z_T\} = Q(z_T) \tag{C-8}$$

and

$$Q(x) = Pr\{X \geq x\} = \frac{1}{\sqrt{2\pi}} \int_x^\infty e^{-t^2/2}\, dt. \tag{C-9}$$

In practice, Y_T is only approximately normal since the mechanisms that give rise to signal fading where $q_T \leq 0.5$ and $z_T \leq 0$ are different from the mechanisms that give rise to signal enhancements where $q_T > 0.5$ and $z_T > 0$. Enhancement is also complicated by ducting phenomena that occur q_D of the time when $z_T > z_D$.

In order to maintain the ease of computation that the standard normal deviate affords, the distribution is divided into three normally distributed segments corresponding to fading, enhancement, and ducting phenomena. Each segment has its own pseudo-standard deviation. The ducting segment has two terms.

The expression for Y_T is

$$Y_T = \begin{cases} \sigma_{T-} z_T, & z_T \leq 0\ (fading) \\ \sigma_{T+} z_T, & 0 < z_T \leq z_D\ (enhancement) \\ \sigma_{T+} z_D + \sigma_{TD}(z_T - z_D), & z_T > z_D\ (ducting) \end{cases} \tag{C-10}$$

where σ_{T-}, σ_{T+}, and σ_{TD} are the fading, enhancement, and ducting pseudo-standard deviations. The pseudo-standard deviations have the ordering $\sigma_{T-} < \sigma_{T+} < \sigma_{TD}$. In other words fading causes the least variation in signal level and ducting the most.

To generate a random A at distance d for Monte Carlo analysis, the parameters μ, σ_{T-}, σ_{T+}, σ_{TD}, and z_D are obtained from the propagation model and the deviate z_T is obtained from a Gaussian random number generator. In the temperate maritime case q_D is 0.9 and z_D is 1.28. The deviate, z_T, is tested to determine whether it is in the fading, enhancement, or ducting regions and the appropriate expression is then used to determine Y_T.

C.1 References

[C-1] P.L. Rice, A.G. Longley, K.A. Norton, and A.P. Barsis,"Transmission loss predictions for tropospheric communication circuits," NBS Technical Note 101, Vol. I, Jan. 1, 1967. http://www.its.bldrdoc.gov/publications/2726.aspx

[C-2] P.L. Rice, A.G. Longley, K.A. Norton, and A.P. Barsis,"Transmission loss predictions for tropospheric communication circuits," NBS Technical Note 101, Vol. II, Jan. 1, 1967, http://www.its.bldrdoc.gov/publications/2727.aspx.

[C-3] A.G. Longley and P.L. Rice, "Prediction of tropospheric radio transmission loss over irregular terrain," ESSA Tech. Report ERL 79-ITS 67, July 1968.

[C-4] G.A. Hufford, A.G. Longley, and W.A. Kissick, "A Guide to the use of the ITS irregular terrain model in the area prediction mode," NTIA Report 82-100, April 1982, http://www.its.bldrdoc.gov/publications/2091.aspx.

APPENDIX D: RADAR SNR

Radar performance is quantified by probability of detection, $\mathcal{P}_d$, and probability of false alarm, $\mathcal{P}_{fa}$. The signal to noise ratio (SNR) required to achieve a performance level is largely determined by the type of integration, i.e., coherent or non-coherent, number of pulses integrated, n_p, and radar cross section (RCS) fluctuation.

This Appendix describes a method for computing the average SNR for non-coherent integration and Swerling1 RCS fluctuation. The method begins with estimating the SNR needed to envelope detect a non-fluctuating target without integration. We then adjust the SNR with estimates of integration gain and fluctuation loss [D-1].

Regarding SNR nomenclature, the SNR for a steady Swerling 0 target before integration is referred to as $\gamma_0(n_p)$ and after integration is $\gamma_0(1)$. Similarly, the average SNR for a fluctuating or Swerling 1 target before integration is $\gamma_1(n_p)$ and after integration is $\gamma_1(1)$. Our goal is to compute $\gamma_1(n_p)$.

For clarity the method is explained in three sections: definitions, intermediate expressions, and final expressions.

D.1 Definitions

We begin with definitions for integration improvement gain, integration loss, and fluctuating loss [D-2]. Integration improvement gain is the gain realized by pulse integration when detecting a steady Swerling 0 target.

$$g_{int}(n_p) \stackrel{\text{def}}{=} \gamma_0(1) \Big/ \gamma_0(n_p). \tag{D-1}$$

The corresponding integration loss is defined as

$$l_{int}(n_p) \stackrel{\text{def}}{=} n_p \Big/ g_{int}(n_p) \tag{D-2}$$

For coherent integration, improvement gain is n_p and therefore lossless.

Fluctuation loss is the loss in detecting a fluctuating target relative to a steady target when the average RCS of the fluctuating target is equivalent to the RCS of the steady target. Without integration it is

$$l_f(1) \stackrel{\text{def}}{=} \gamma_1(1) \Big/ \gamma_0(1) \tag{D-3}$$

and with integration it is

$$l_f(n_p) \stackrel{\text{def}}{=} \gamma_1(n_p) \Big/ \gamma_0(n_p). \tag{D-4}$$

D.2 Intermediate Expressions

We have at our disposal expressions for $\gamma_0(1)$, $\gamma_1(1)$, $g_{int}(n_p)$, and $l_f(n_p)$ which can be used in conjunction with the definitions above to solve for $\gamma_1(n_p)$. The SNR needed to envelope detect a non-fluctuating target without integration, $\gamma_0(1)$, can be estimated with the empirically derived expression [D-3]

$$\gamma_0(1) = A + 0.12AB + 1.7B \tag{D-5}$$

where $A = \ln[0.62/\mathcal{P}_{fa}]$ and $B = \ln[\mathcal{P}_d/(1-\mathcal{P}_d)]$. This expression is accurate to within 0.2 dB for $\mathcal{P}_{fa}$ between 10^{-3} and 10^{-7}, and $\mathcal{P}_d$ between 0.1 and 0.9.

The average SNR, $\gamma_1(1)$, can be determined from the exact solution for a Swerling 1 target without integration by [D-2]

$$\mathcal{P}_d = e^{\frac{\ln(\mathcal{P}_{fa})}{(1+\gamma_1(1))}}. \tag{D-6}$$

Rearranging terms

$$\gamma_1(1) = \frac{\ln(\mathcal{P}_{fa})}{\ln(\mathcal{P}_d)} - 1. \tag{D-7}$$

The integration improvement gain, $g_{int}(n_p)$, for non-coherent integration and a Swerling 0 target can be estimated with the empirically derived approximation [D-4]

$$G_{int}(n_p) = 6.79[1 + 0.253\mathcal{P}_d]\left[1 + \frac{\log_{10}\left(1/\mathcal{P}_{fa}\right)}{46.6}\right]\log_{10}(n_p)\left[1 - 0.14\log_{10}(n_p) + 0.0183\left(\log_{10}(n_p)\right)^2\right] \ (dB) \tag{D-8}$$

where $G_{int}(n_p) = 10\log_{10} g_{int}(n_p)$. This approximation is accurate to within 0.8 dB for $\mathcal{P}_{fa}$ = 10^{-2}, 10^{-4}, 10^{-6}, 10^{-8}, and 10^{-10} for all values of $\mathcal{P}_d$ = 0.5, 0.7, 0.9, 0.99, and 0.999 and n_p = 1, 3, 10, 30, and 100.

And finally, the fluctuation loss with integration relative to the fluctuation loss without integration for the Swerling 1 targets is [D-2]

$$l_f(n_p) = l_f(1)^{(1+\alpha)} \tag{D-9}$$

or

$$l_f(n_p) = \left[\gamma_1(1) \Big/ \gamma_0(1) \right]^{(1+\alpha)} \tag{D-10}$$

where $\alpha = 0.035 \log_{10}(n_p)$.

D.3 Final Expressions

We will now show how the definitions and intermediate expressions can be used to solve for the SNR before integration, $\gamma_1(n_p)$. Beginning with (D-4)

$$\gamma_1(n_p) = \gamma_0(n_p) l_f(n_p) \tag{D-11}$$

then

$$\gamma_1(n_p) = \frac{\gamma_0(1) l_f(n_p)}{g_{int}(n_p)} \tag{D-12}$$

or

$$\gamma_1(n_p) = \frac{\gamma_0(1) l_{int}(n_p) l_f(n_p)}{n_p} \tag{D-13}$$

Performance for the radar in this report, calculated with this method, is shown in Figure D-1. The figure shows that the average SNR for $\mathcal{P}_d$ = 0.8 and $\mathcal{P}_{fa}$ = 10^{-4} is 10.0 and 7.6 dB for 6 and 14 non-coherently integrated pulses, respectively.

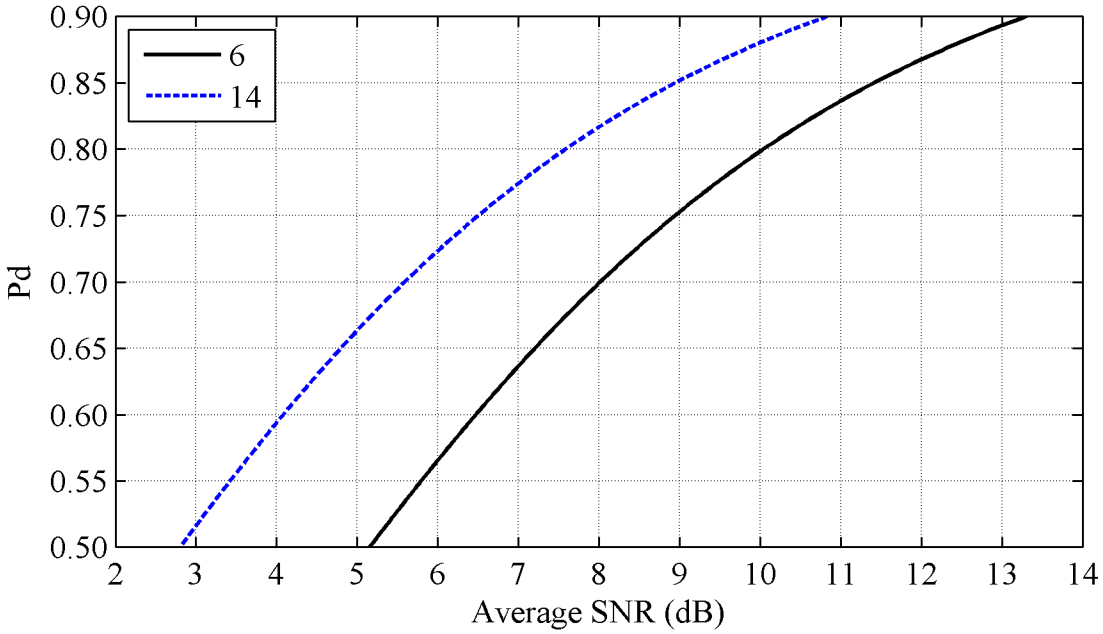

Figure D-1. Radar $\mathcal{P}_d$ with Swerling 1 target, non-coherent integration of 6 and 14 pulses, and 10^{-4} $\mathcal{P}_{fa}$.

D.4 Other Considerations

The SNR, $\gamma_1(n_p)$, is the SNR required at the input to the receiver without signal processing losses. With signal processing losses, l_{sp}, the SNR required at the input to the receiver is

$$w = \gamma_1(n_p) l_{sp} \tag{D-14}$$

or

$$w = \frac{\gamma_0(1) l_{int}(n_p) l_f(n_p) l_{sp}}{n_p} \tag{D-15}$$

Possible sources of processing loss include one or more of the following: the IF filter not being matched to the transmitted pulse shape, the digitizer missing the highest signal, or the constant false alarm rate function misestimating the detection threshold.

D.5 References

[D-1] D.K. Barton, "Simple procedures for radar detection calculations," *IEEE Trans. On Aerospace and Electronic Systems*, Vol. AES-5, No. 5, Sept. 1969, pp. 837-846.

[D-2] D.K. Barton, "Theory of Target Detection" in *Radar System Analysis and Modeling*, Artech House, Boston, MA, 2005.

[D-3] M.L. Skolnik, “The radar equation,” Chapter 2 in *Introduction to Radar Systems*, Third Edition, McGraw Hill, New York, N.Y., 2001.

[D-4] P.Z. Peebles, *Radar Principles*, John Wiley Inc., New York, N.Y., 1998, pp. 401-402.

NTIA FORM 29
(4-80)

U.S. DEPARTMENT OF COMMERCE
NATIONAL TELECOMMUNICATIONS AND INFORMATION ADMINISTRATION

BIBLIOGRAPHIC DATA SHEET

1. PUBLICATION NO.	2. Government Accession No.	3. Recipient's Accession No.
TR-15-513		

4. TITLE AND SUBTITLE	5. Publication Date
Effect of Broadband Radio Service Reallocation on 2900–3100 MHz band Marine Radars: Background	April 2015
	6. Performing Organization Code NTIA/ITS.T

7. AUTHOR(S)	9. Project/Task/Work Unit No.
Robert Achatz, Paul McKenna, Roger Dalke, Nicholas DeMinco, Frank Sanders, John Carroll	3105011-300
8. PERFORMING ORGANIZATION NAME AND ADDRESS Institute for Telecommunication Sciences National Telecommunications & Information Administration U.S. Department of Commerce 325 Broadway Boulder, CO 80305	10. Contract/Grant Number.
11. Sponsoring Organization Name and Address U.S. Coast Guard Spectrum Management Telecommunications Policy Division U.S. Coast Guard CG-652, 2100 2nd St. SW Stop 7101 Washington, DC 20593-7101	12. Type of Report and Period Covered

14. SUPPLEMENTARY NOTES

15. ABSTRACT (A 200-word or less factual summary of most significant information. If document includes a significant bibliography or literature survey, mention it here.)

Spectrum reallocations may place broadband radio services (BRS) near spectrum used by 2900–3100 MHz band marine radars. Interference effects from these reallocations include unwanted emissions in the radar detection bandwidth and front-end overload. This report provides background information for subsequent reports that analyze these effects. Interference protection criteria (IPC) are identified, an interference scenario is described, and models for the radar system, BRS system, radar target, and radio wave propagation are presented. The BRS signal is shown to be reasonably emulated by Gaussian noise. A method for determining the aggregate power distribution using a realistic propagation model and Monte Carlo analysis is described. The aggregate power from the base stations was found to be as much as 6 dB more than power from a single base station. Finally a method for incorporating a variable SNR, caused by variable radar to target path loss, into interference analysis is shown.

16. Key Words (Alphabetical order, separated by semicolons)
aggregate power, broadband radio service, front-end overload, interference, interference protection criteria, marine radar, radar, radio spectrum engineering, radio wave propagation, signal characterization, unwanted emissions

17. AVAILABILITY STATEMENT	18. Security Class. (This report)	20. Number of pages
☒ UNLIMITED.	Unclassified	87
☐ FOR OFFICIAL DISTRIBUTION.	19. Security Class. (This page)	21. Price:
	Unclassified	N/A

NTIA FORMAL PUBLICATION SERIES

NTIA MONOGRAPH (MG)

A scholarly, professionally oriented publication dealing with state-of-the-art research or an authoritative treatment of a broad area. Expected to have long-lasting value.

NTIA SPECIAL PUBLICATION (SP)

Conference proceedings, bibliographies, selected speeches, course and instructional materials, directories, and major studies mandated by Congress.

NTIA REPORT (TR)

Important contributions to existing knowledge of less breadth than a monograph, such as results of completed projects and major activities.

JOINT NTIA/OTHER-AGENCY REPORT (JR)

This report receives both local NTIA and other agency review. Both agencies' logos and report series numbering appear on the cover.

NTIA SOFTWARE & DATA PRODUCTS (SD)

Software such as programs, test data, and sound/video files. This series can be used to transfer technology to U.S. industry.

NTIA HANDBOOK (HB)

Information pertaining to technical procedures, reference and data guides, and formal user's manuals that are expected to be pertinent for a long time.

NTIA TECHNICAL MEMORANDUM (TM)

Technical information typically of less breadth than an NTIA Report. The series includes data, preliminary project results, and information for a specific, limited audience.

For information about NTIA publications, contact the NTIA/ITS Technical Publications Office at 325 Broadway, Boulder, CO, 80305 Tel. (303) 497-3572 or e-mail info@its.bldrdoc.gov.